PHYSICAL REVIEW C VOLUME 53, NUMBER 3 MARCH 1996

ARTICLES

Pion absorption on ^{3}He at low energies

H. Hahn,[1] A. Altman,[2] D. Ashery,[1] G. Gefen,[1] D. R. Gill,[2] R. R. Johnson,[2,3] R. Levy-Nathansohn,[1] M. A. Moinester,[1]
M. Sevior,[2] and R. P. Trelle[3]

[1]*Raymond and Beverly Sackler Faculty of Exact Sciences,*
School of Physics and Astronomy, Tel Aviv University, 69978 Ramat Aviv, Israel
[2]*TRIUMF, 4004 Wesbrook Mall, Vancouver, British Columbia, Canada V6T 2A3*
[3]*Department of Physics, University of British Columbia, Vancouver, British Columbia, Canada V6T 2A6*

(Received 28 November 1994; revised manuscript received 5 December 1994)

The reactions ^{3}He$(\pi^+,pp)p$ and ^{3}He$(\pi^-,pn)n$ were studied at 37.0 MeV by coincidence detection of two nucleons. The differential cross sections were separated to two-nucleon (σ_{2N}), three-nucleon (σ_{3N}), and final-state interaction ($\sigma_{\rm FSI}$) components. For π^+, the σ_{2N} angular distribution is symmetric about 90°, and the total cross section is 1.5 times the cross section measured for $d(\pi^+,pp)$. For π^-, the angular distribution is asymmetric (backward peaked). The asymmetry increases with decreasing energy, indicating increasing pion s-wave contribution at lower energies. The fraction of the cross section induced by s-wave pions as calculated by a partial wave amplitude analysis is 13%. The measured total cross sections are $\sigma_{2N}(\pi^-)=0.85\pm0.08$ mb and $\sigma_{2N}(\pi^+)=7.9\pm0.5$ mb; $\sigma_{3N}(\pi^-)=1.6\pm0.7$ mb and $\sigma_{3N}(\pi^+)=1.3\pm0.3$ mb. A new evaluation of σ_{3N} at $T_\pi=62.5$ and 82.8 MeV is given, using data from an earlier experiment. The cross sections leading to the two-nucleon final-state interaction at $T_\pi=37.0$ MeV are also estimated.

PACS number(s): 25.80.Ls, 21.45.+v

I. INTRODUCTION

The motivations and objectives in studying pion absorption on ^{3}He can be classified as follows: Study of pion absorption on a $T=0$ nucleon pair. Comparison with pion absorption on the deuteron yields information on the nuclear density dependence of the process. Study of pion absorption on a $T=1$ nucleon pair. Study of pion absorption on three nucleons.

It is of great interest to study the behavior of nucleon interactions at distances equal to or shorter than their diameter. At such ranges we can expect some transition from the well-described "nucleon sector" of long range interaction mediated by meson exchange to a "quark sector" where the nucleon internal degrees of freedom may become recognizable. Some suggested descriptions of this sector as, e.g., a "six-quark bag" exist. The short range repulsion generated by the color hyperfine interaction [1] makes the probability for such a component in the two-nucleon wave function very small. Whether this description or any other one is relevant has to be decided through experimental observables.

The two-nucleon potential is derived from phase-shift analysis of nucleon-nucleon scattering and reactions. For bound nucleons at short distances this requires s-wave phase shifts derived from large momentum transfer and small scattering angle measurements which are hard to obtain experimentally. Consequently, different potentials which all fit well the experimental phase shifts result in a variety of two-nucleon correlation functions which are in serious disagreement at short ranges. As an illustration, two such correlation functions for the $T=0$ nucleon pair in ^{3}He are shown in Fig. 1. One is based on the Reid soft core potential [2] and the other on the Argonne v_{14} potential [3].

It is therefore important to search for other experimental observables that will be sensitive to the behavior of nucleons at short ranges. Pion absorption is a high momentum transfer process (>350 MeV/c), it involves more than one nucleon, and hence can provide sensitivity to small distances between the absorbing nucleons ($0.5-0.7$ fm). A natural testing ground is found in the lightest nuclei: the deuteron, ^{3}He, and ^{4}He with charge radii of 2.1, 1.85, and 1.68 fm, respectively [4]. This corresponds to a relative average nucleon density ratio of 1:2.2:3.9. An observable sensitive to short range correlations should show significant nontrivial variation when

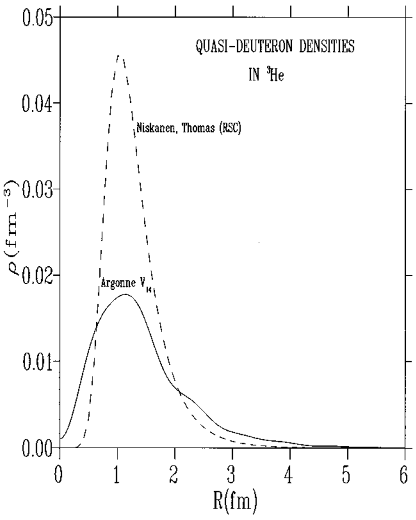

FIG. 1. Correlation functions for the quasideuteron in ^{3}He [2,3].

0556-2813/96/53(3)/1074(18)/$10.00

compared among these three nuclei.

The pion absorption process is, however, dominated by the p-wave pion rescattering diagram in which the Δ resonance is created in the intermediate state. Absorption occurs by a $\Delta N \to NN$ process with the (ΔN) system in a relative $L=0$. This mechanism masks the $N-N$ correlations due to the long range nature of the Δ-mediated pion absorption process [5]. Indeed, cross section measurements of π^+ absorption on ^{3}He and ^{4}He showed no sensitivity to short range $N-N$ correlations [6,7] as may be evidenced by observation that for all angles,

$$\sigma(\pi^+ ``d" \to pp) \cong N_{``d"} \cdot \sigma(\pi^+ d \to pp), \tag{1}$$

where $N_{``d"}$ is the number of $T=0$ pn pairs (quasideuterons) in the nucleus. The conclusion is that *in order to study short range nucleon correlations the observables must be sensitive to components of pion absorption where the* Δ *resonance is not dominant*.

Recently, a connection was established between the s-wave rescattering term in pion absorption and the axial exchange-charge operator which is derived from nuclear β decay [8]. This was also simulated through heavy meson exchange [9], and it becomes a very useful tool to study short range correlations. The experimental determination of the s-wave rescattering term can be done either through measurements of spin observables [10,11], or by studying pion absorption at low energies.

For π^- absorption on the diproton, the $J^\pi = 0^+$, $T=1$ quantum numbers generate simple selection rules for this reaction: the total spin parity is always unnatural, and therefore the final two nucleons (pn) are in the triplet $(S=1)$ state. Consequently, even pion partial waves lead to negative parity, and hence to total isospin $T=1$. Odd partial waves lead to positive parity and $T=0$. For the $T=1$ channel, which allows an intermediate Δ to be produced, the negative parity does not allow the $\Delta - N$ system to be in relative $L=0$. This reduces the probability of finding the Δ and the nucleon close enough for absorption to take place, and this channel will proceed mainly through non-Δ s-wave rescattering. Under these circumstances the $T=0$ channel, where the Δ cannot play any role, may become dominant. Absorption in this channel may take place directly on the two protons, and, unlike pion absorption on a $T=0$ nucleon pair, it may be sensitive to their short range correlation function.

Measurements of this process through studies of the $^3\mathrm{He}(\pi^-,pn)n$ reaction were performed in the past for bombarding energies of 63–350 MeV [12–17]. It is interesting to note that the cross section for the $^4\mathrm{He}(\pi^-,pn)nn$ reaction was found [7] to be about 1.7 times larger than that for ^{3}He. Since the number of diprotons is the same in both nuclei this may be an indication that this reaction is indeed sensitive to the short range correlations of the two protons: the nucleon density of ^{4}He is twice that of ^{3}He.

At low energies one may assume that only s- and p-wave pions contribute. Analysis of the angular distributions shows that the reaction is dominated by the p-wave pions, $T=0$ (non-Δ) transition [13]. A more detailed analysis [18] concludes that this $T=0$ component has two possible final pn states: about equal ^3S and ^3D, or mostly ^3D. A complete determination of all transition amplitudes can be reached by measuring the polarization of one outgoing nucleon [19–21]. Two of the assumptions made in these analyses become better justified at low energies: the assumption that only s- and p-wave pions contribute, and the application of the Watson theorem done in [18,19]. At these energies also the Δ resonance plays a smaller role, and it is easier to identify the s-wave rescattering term which is sensitive to short range correlations. It is therefore of interest to study pion absorption in ^{3}He at as low energies as possible. We report here the results of pion absorption studies done at the lowest bombarding energy so far: 37.0 MeV.

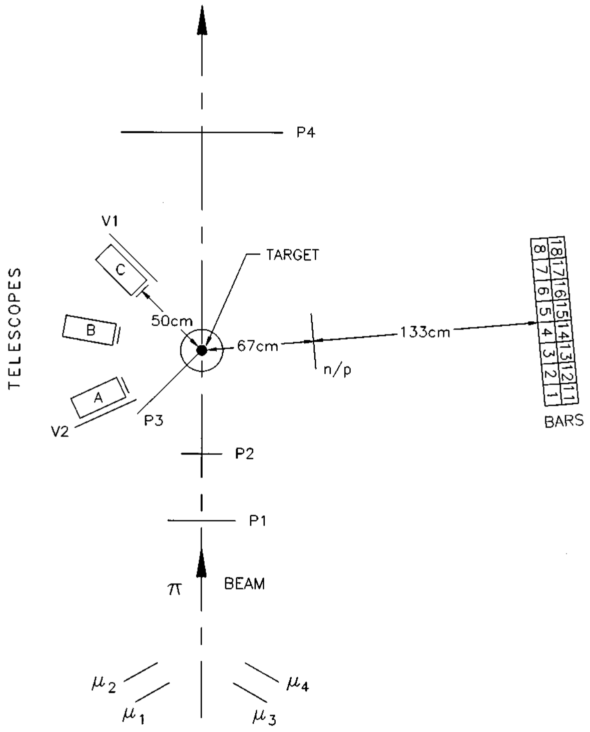

FIG. 2. General layout of the experiment.

In pion absorption on ^{3}He, the three nucleons in the final state may emerge with comparable momenta. This *three-nucleon* $(3N)$ *absorption* is observed over all the available phase space. Experimentally, two special kinematical situations are found to be enhanced in the absorption process: the *two-nucleon* $(2N)$ *absorption* and the so-called *"soft" final-state interaction* (FSI). The $2N$ absorption is defined by two nucleons sharing all the available momentum between them. The third nucleon then acts as a *spectator* only, gaining no additional momentum over the Fermi momentum it initially had in the nucleus. The $2N$ absorption is identified by the combination of two closely related experimental signatures: (a) the angular correlation at which the two absorbing nucleons are observed (around 180° c.m., with a spread caused by the Fermi momentum), and (b) the momentum of the spectator nucleon, $p_3 \leqslant 150$ MeV/c. Up to this momentum limit, the spectator momentum distribution in the absorption process (see Fig. 7) follows the momentum distribution observed in breakup experiments [22,23] of ^{3}He. Apart from the spread due to the Fermi momentum, the kinematics of this $2N$ absorption are identical to the kinematics of the $d(\pi^+,pp)$ reaction.

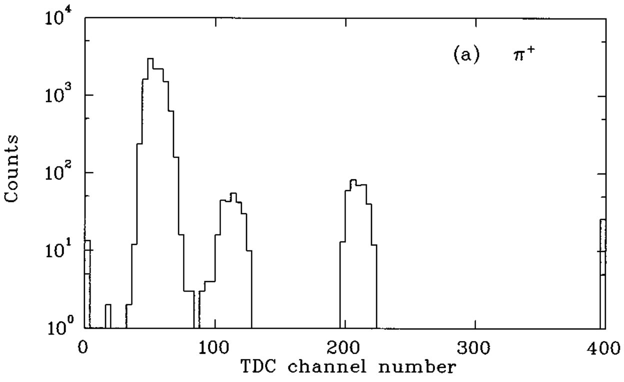

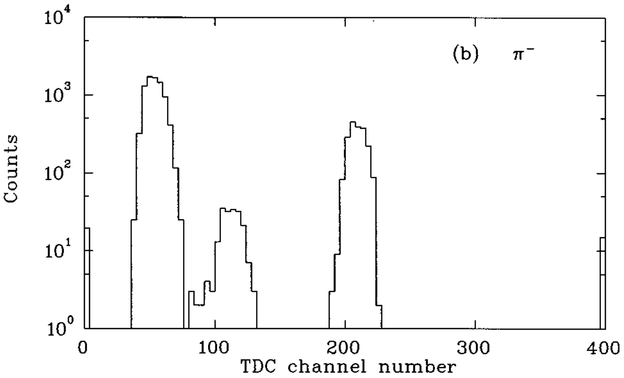

FIG. 3. Two examples of the TDC spectrum of the beam, showing the beam composition for π^+ (a) and π^- (b). The peaks are (from left to right) from pions, muons, and electrons. The calculation of the pion fraction of the beam is based on the ratio of peak areas (or counts).

The second of the enhanced processes, the FSI, is defined by two nucleons interacting in the final state and recoiling together at 180° c.m. with respect to the third nucleon. In contrast to the $2N$ absorption case, all three nucleons gain considerable momentum, with the single nucleon which recoils against the pair gaining the highest momentum available in the absorption process. This FSI is of increasing significance at lower energies and was clearly observed with stopped pions [24]. Its contribution was also strongly felt in the present experiment.

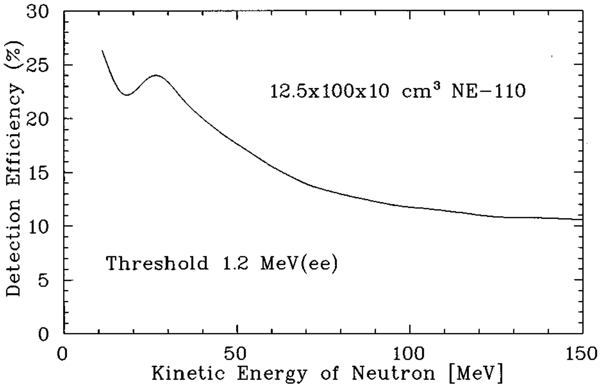

FIG. 4. Neutron detection efficiency for one layer of the bars, averaged over bar 1 (at the edge of the wall) and bar 4 (at the center).

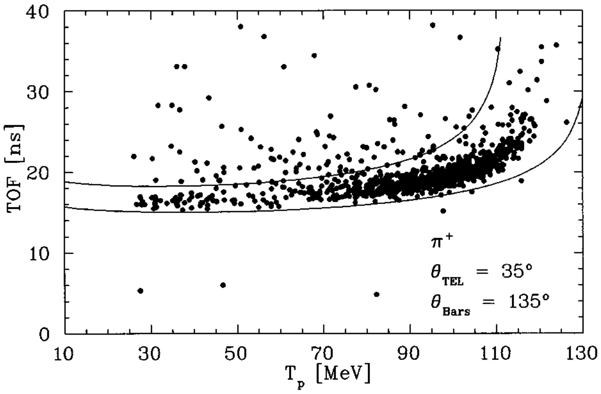

FIG. 5. Example of the kinematic bands, with the detectors at conjugate angles.

In the following sections we present the results of $2N$, $3N$, and FSI π^+ and π^- absorption on ^{3}He at 37.0 MeV. We also include a new evaluation of the $3N$ absorption (π^+ and π^-) at 62.5 and 82.8 MeV, based on the data of Aniol *et al.* [13].

II. EXPERIMENT

The experiment was performed at the M13 channel of TRIUMF. The general layout of the experiment is shown in Fig. 2. To the left of the beam, three NaI scintillators (*"telescopes"*) were placed for proton detection. To the right, a plastic scintillator wall (the *"bars"*) served for the detection of a second proton when using the π^+ beam, and for neutron detection when using the π^- beam. The bars could be moved with their center located between 35° and 135° with respect to the nominal beam direction. The telescopes could be moved from 35° to 120°, with the angular separation between them fixed at 30°. The beam passed between two pairs of small detectors $\mu_1 - \mu_4$, arranged symmetrically on both sides. They monitored the beam by detecting muons resulting from pion decay in flight. Correct central setting of the beam was checked by symmetry in the counting rates of these detectors. The in-beam scintillators $P1$ and $P2$ counted the beam rate. The scintillators $P3$, $V1$, and $V2$ were used to

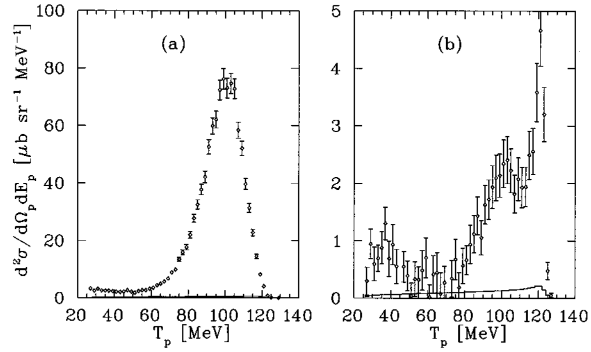

FIG. 6. Energy spectra of the telescopes for $\theta_{TEL} = 35°$, $\theta_{bars} = 135°$ (conjugate angles), (a) π^+, and (b) π^-. Plotted are $N_1 - N_2 - K(N_3 - N_4)$, transformed into doubly differential cross sections by Eq. (12) (data points), and the $3N$ absorption phase space normalized by off-conjugate measurements (solid line).

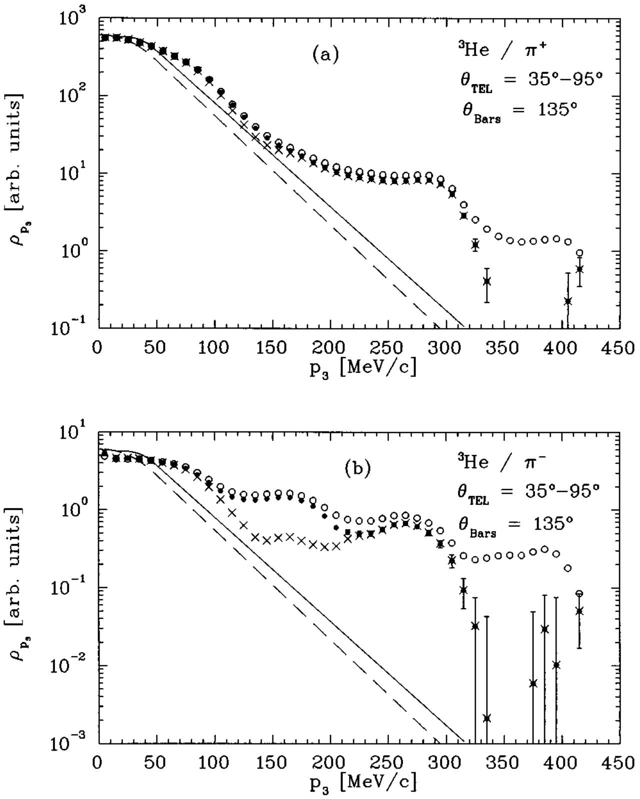

FIG. 7. The momentum density distribution ρ_{p_3} of the undetected nucleon. Solid line (dashed line), results for $ppn(pd)$ breakup, of ^{3}He with electrons as measured by Jans *et al.* [23]. Open circles, momentum distribution from data. Solid circles, momentum distribution after subtracting the calculated $3N$ contribution from the data. Crosses, correction to solid circles after subtracting part of the FSI (region I in Fig. 8). (a) π^+, (b) π^-, at the same angular combinations.

exclude counts from scattered particles. The n/p plastic scintillator (thickness 3.175 mm), covering the solid angle of the bars, served for discrimination of charged particles.

The target was liquid ^{3}He, contained in a cylindrical vessel similar to the one described by Aniol *et al.* [13], but with a smaller diameter (50.8 mm). The temperature was kept constant at 1.68 ± 0.01 K. The temperature uncertainty corresponds to a density variation of less than 10^{-3}. The effective target thickness of $(7.74\pm0.15)\times10^{22}$ cm^{-2} was calculated by convoluting the measured beam profile with the target shape. The uncertainty includes the effects of target thickness variations over the beam profile. The density of ^{3}He at this temperature is $\rho=79.6$ mg/cm^3. An identical but empty target vessel was used in empty-target runs for the subtraction of background from the target walls.

Each telescope consisted of a very thin plastic scintillator (ΔE: 1.6 mm, with 10.2 cm diameter), followed by the NaI scintillator (E) of 12.7 cm diameter. The combination of ΔE and E information allowed particle identification (pions, protons, deuterons). Each telescope covered a solid angle of 32.4 ± 1.3 msr. The energy resolution of the NaI scintillators was 2.8 MeV FWHM at $T_p=66$ MeV, increasing to 4.3 MeV at $T_p=98$ MeV.

The plastic scintillator (bars) array was composed of 16 bars of plastic scintillators (NE 110, with an attenuation length of >4 m), arranged in two layers of eight bars each. Each bar measured $12.5\times10.0\times100.0$ cm^3, giving two walls of 100×100 cm^2 front area and 10 cm thickness each. The distance of the central point of the bars front to the center of the target was 200 cm. The two walls were arranged one directly behind the other to yield a total thickness of 20 cm, for optimization of the neutron detection efficiency. Each bar was equipped with phototubes at its top and bottom. Their detection threshold was set at the Compton edge of the γ rays of a ^{60}Co source (≈1.0 MeV). Including electron contributions and attenuation length corrections, this threshold setting equals 1.2 MeV *electron equivalent (ee)*. The neutron detection efficiency correction (Sec. III) is based on this threshold. The sum of the top and bottom TDC's (started by $P2$) was used to measure the time of flight (TOF) of the particle, with a resolution of 0.8 ns (FWHM). From the time difference between top and bottom TDC's, the position of the event along the bar was calculated. The resolution of the vertical position was about 6 cm FWHM. Horizontally, the position resolution was determined by the width of the bars (12.5 cm).

TABLE I. Angular settings for pion absorption measurements.

Conjugate telescope	Conj. $\theta_{\mathrm{TEL}(1)}$	θ_{bar}	Nonconjugate $\theta_{\mathrm{TEL}(2)}$	$\theta_{\mathrm{TEL}(3)}$
C	35.0°	135.0°	65.0°	95.0°
C	50.0°	118.0°	80.0°	110.0°
B	65.0°	101.0°	35.0°	95.0°
B	80.0°	85.0°	50.0°	110.0°
A	100.0°	66.0°	40.0°	70.0°
A	120.0°	48.0°	60.0°	90.0°

In the electronics, an event was defined by coincidence between one (or more) bars and at least one of the telescopes (each telescope itself being defined by $\Delta E\cdot E$). An anticoincidence with the n/p detector (see Fig. 2) was required to exclude charged particles in the bars (for π^- runs only). In addition, the combination $P1\cdot P2\cdot\overline{P3}\cdot\overline{(V1+V2)}$ was required for a real beam event. The number of beam particles satisfying this requirement was defined as the *beam counts*, Φ. This number was corrected for dead time by the electronic setup.

The kinetic energy of the beam at the target center (after energy loss corrections) was $T_\pi=37.0\pm0.5$ MeV. Beam samples were used to check the pion fraction of the beam, by measuring the time of flight between the rf signal of the cyclotron and scintillator $P2$ (see Fig. 3). In this way, beam contaminations by electrons and muons could be determined. The fraction of muons from pion decay upstream of the $P2$ detector, misidentified as pions, was estimated using the calculations of [25]. The pion fraction f_π was 0.94 ± 0.01 for the π^+ beam. For the π^- beam, f_π was 0.71 and 0.76 (with Be and C production targets, respectively), and was measured with an uncertainty $\Delta f_\pi<0.01$.

The differential cross sections for the $2N$ absorption processes ^{3}He$(\pi^+,pp)p$ and ^{3}He$(\pi^-,pn)n$ were measured at six angular combinations (Table I), selected by the kinematics of the free $2N$ absorption process $d(\pi^+,pp)$ (the *"conjugate angles"*). At each of these six angular combinations, the two additional telescopes (cf. Fig. 2) were used for data taking at *"nonconjugate angles,"* measuring $3N$ absorption, at 12 angular combinations. Eight of them had the telescopes at an angular separation of 30° from the conjugate angle (*"30° off conjugate"*), four at *"60° off conjugate"* (see Table I).

Each measurement was repeated with the empty-target vessel. Telescope singles runs (runs for which an event is defined when a charged particle hits one of the telescopes, without requiring coincidence with the bars) were taken at three telescope settings with the π^+ beam, yielding singles spectra at nine angles, and at two settings (six angles) with the π^- beam. The singles runs with the π^+ beam were repeated with empty target. For the π^- beam, the two-body reaction $^3\mathrm{He}(\pi^-,\mathrm{d})\mathrm{n}$ could be observed in both the singles runs and coincidence runs at conjugate angles by using the telescopes for identification of the deuterons. CH_2 and CD_2 targets (and C targets for background subtraction) were used for energy calibration and as a check on the experimental apparatus by comparison with known $d(\pi^+,pp)$ cross sections. Our measured cross section for this reaction (5.9 ± 0.5 mb) is consistent with the results of [26].

III. ANALYSIS

A. Calibration and calculation of yield

The energy calibration of the telescopes was done using known proton and pion energies from $d(\pi^+,pp)$ and $\pi p\rightarrow\pi p$ reactions. The energy of the detected particle in the telescope was corrected for energy losses between the event vertex and the telescope. The threshold at the event vertex, corresponding to a detected proton energy of $E_{\mathrm{TEL}}\geqslant6.2$ MeV, was at $E_1\geqslant26.0$ MeV. A correction was made for the effect of protons reacting in the NaI detector. This correction, based on the measurements of [27], was done by deconvoluting the spectrum channel by channel, beginning with the highest energy channel. Corrections were of the order of 10% for the highest proton energies, going down to zero at the low energy end.

The time-of-flight calibration of the protons to the bars was done similarly, assuming interaction at the bars front and including corrections for energy losses between the event vertex and the bars. For the neutrons, no energy losses had to be taken into account, and the distance was taken to the center of the interacting bar. The threshold for the acceptance of protons and neutrons in the bars was set by TOF considerations (TOF $\leqslant35$ ns), corresponding to a proton energy of $E_2\geqslant34$ MeV and a neutron energy of $E_2\geqslant18$ MeV.

The total energy was determined by the target mass and the incident beam energy. Measuring the momentum of the proton in the telescope and the angles at which the nucleon is detected in the bars is sufficient to allow the calculation of the momenta and energies of the second and third final-state particles from three-body kinematics. The additional measurement of the momentum of the nucleon in the bars results therefore in an overdetermination of the kinematics, which was used for cross checks and background reduction. The TOF of the nucleon to the bars was calculated and compared to the measured TOF. Differences showed a Gaussian distribution with a standard deviation of typically <1 ns and negligible deviations of the peak from zero.

The neutron detection efficiency of the bars was calculated with the Kent State Monte Carlo code [28], with 1.2 MeV *(ee)* threshold. The result (for one layer of bars) is shown in Fig. 4. The uncertainty in the calculation of the neutron detection efficiency, including averaging over central and outermost bars, is about 6%. The neutron detection efficiency was checked by comparing the yield of the reaction $^3\mathrm{He}(\pi^-,dn)$ in telescope singles runs with the yield in coincidence runs, using the above efficiency correction for the bars. The results were consistent.

From these data, a scatter plot was formed of the time-of-flight TOF_N of the nucleon to the bars versus the energy E_1 of the proton detected by the telescope, both corrected to the target's center (Fig. 5). The two lines were calculated from the kinematics of the reaction and the resolution of the detectors. Only events falling within the kinematic band were accepted for the analysis. Below the band are events from random coincidences only; above it, additional events from pion absorption in heavier nuclei in the target walls are observed. The figure shows the data of all the bars added together. In the actual analysis, the kinematic band was calculated for each bar separately, leading to narrower bands for the special kinematic conditions of each bar.

Multiple hits in the bars were sorted out by first checking whether two counts could be related to one nucleon. If they were observed in two neighboring bars or in a front-back pair of bars and at the same height (to within ±6 cm), they were handled as originating from one nucleon. If, at the end of this sorting, two independent hits remained, and if both were in the kinematic band, they were marked in the data file as a double hit and counted as one event. Double hits in the telescopes (two protons reaching two different telescopes simultaneously) were not observed at all. This demonstrates that vetoing of good events by a third proton hitting the $P3$ or $V1$ or $V2$ veto detectors is negligible.

Random coincidence contributions were subtracted by defining a band of equal shape and area as the kinematic band, in the area of shorter TOF (the random band), and subtracting the events in the random band (N_2) from the events in the kinematic band (N_1). The ratio N_2/N_1 varied between <0.01 for π^+ at conjugate angles and ≈0.5 for π^- at angles 60° off conjugate. The same procedure was repeated for empty-target runs, to correct for contributions from the target walls. The ratio of events observed in the kinematic bands of the empty and the full target, N_3/N_1, varied in the same range as N_2/N_1. For empty-target runs, the difference between events in the kinematic band (N_3) and in the random band (N_4) fluctuated around zero. This net number of empty-target events was normalized to the beam counts Φ_{full} of the full target run. Defining $K=\Phi_{\mathrm{full}}/\Phi_{\mathrm{empty}}$, the net number of events is given by

$$N=N_1-N_2-K(N_3-N_4), \tag{2}$$

with the error ΔN given by

$$\Delta N=\sqrt{(\Delta N_1)^2+(\Delta N_2)^2+K^2[(\Delta N_3)^2+(\Delta N_4)^2]}. \tag{3}$$

For π^- runs, each N_i ($i=1,\ldots,4$) was corrected for the neutron detection efficiency η, as discussed above. If N_i'

designates the uncorrected number of events, then $N_i = N_i'/\eta$. Therefore, each ΔN_i of Eq. 3 is given by

$$\Delta N_i = \sqrt{\frac{N_i}{\eta} + \left(\frac{\Delta \eta}{\eta} N_i \right)^2}, \tag{4}$$

where we made use of the relations $N_i = N_i'/\eta$ and $(\Delta N_i')^2 = N_i'$.

B. Three-nucleon absorption cross sections

The net number of counts given by Eq. 2 was transformed into triply differential cross sections by

$$\frac{d^3\sigma}{dE_1 d\Omega_1 d\Omega_2} = \frac{N_{E_1}}{\Delta\Omega_1 \Delta\Omega_2 \Phi f_\pi N_{\mathrm{tgt}}}. \tag{5}$$

Here N_{E_1} is the number of counts *per MeV* of the protons detected in the telescope, $\Delta\Omega_1$ the solid angle of the telescope, Φ the number of incident beam particles, f_π the pion fraction of the beam, N_{tgt} the number of ^{3}He nuclei per unit area, and $\Delta\Omega_2$ the angular opening of the bars.

We assume a phase-space-like behavior of the $3N$ absorption at all nonconjugate angles. This assumption was found to be approximately correct in previous experiments [13] as well as in the present one. In particular, this was confirmed by a recent experiment [29] in which a large fraction of phase space was studied. In this case, the matrix element connecting the phase space to the differential cross section will be constant. We denote it by the factor f to be found experimentally:

$$\frac{d^3\sigma}{dE_1 d\Omega_1 d\Omega_2} = f \frac{d^3 R}{dE_1 d\Omega_1 d\Omega_2}. \tag{6}$$

The phase space was calculated under the experimental conditions (detector acceptances, energy thresholds) by the formula (see [30,31])

$$\frac{d^3 R}{dE_1 d\Omega_1 d\Omega_2} = \frac{p_1 p_2^2}{8[E_3 p_2 + E_2(p_2 - p\cos\theta_2 + p_1 \cos\theta_{1,2})]}. \tag{7}$$

The subscripts 1,2,3 denote the proton detected in the telescope, the nucleon detected in the bars, and the undetected nucleon, respectively. Here, $\theta_{1,2}$ is the angle between the proton detected in the telescope and the nucleon detected in the bars, and p is the momentum of the pion.

For both data and phase-space calculations, a cut was made on the recoil momentum of the undetected nucleon. Requiring $p_3 \geqslant 200$ MeV/c (for the purpose of determining the factor f) excluded significant $2N$ reaction contributions. In the present experiment, large FSI contributions were observed at the conjugate angles, and could be observed even at configurations 30° off conjugate in the four or five bars nearest the conjugate angle. Therefore, for the eight configurations 30° off conjugate, only the three remaining bars farthest from the conjugate angle, showing no FSI influence, were used for calculation of the $3N$ phase-space normalization. For the four configurations 60° off-conjugate angle, all eight bars were used. Thus, out of the 12 off conjugate angular combinations listed in Table I, eight were with the bars centered at $\approx 40°$ off conjugate and an angular opening of 10.7°, and four with the bars centered at $\approx 60°$ off conjugate and an angular opening of 28.6°. The phase-space expressions were then normalized to the data at these 12 points by a least squares fit. The normalization yielded the factor f defined in Eq. (6) at the 12 angular combinations (see Table III in Sec. IV C).

The average factor $\langle f \rangle$ found in this way was then used to calculate the total $3N$ absorption cross section. By integrating phase space over all angles and the allowed energy range, we get the total $3N$ phase space:

$$R_3 = \int_0^{p_{1,\max}} \frac{d^3 p_1}{2E_1} R_2(|Q|, m_2, m_3), \tag{8}$$

where $R_2(|Q|, m_2, m_3)$, the two-body phase space, is given by

$$R_2(|Q|, m_2, m_3) = \frac{\pi[Q^4 - 2Q^2(m_2^2 + m_3^2) + (m_2^2 - m_3^2)^2]^{1/2}}{2Q^2} \tag{9}$$

(see [31]; Q is the combined four-momentum of nucleons 2 and 3). Multiplying the total $3N$ phase space by $\langle f \rangle$, we got the total $3N$ cross sections:

$$\sigma_{3N,\pi^+} = \frac{f_{\pi^+}}{3!} R_3, \tag{10}$$

$$\sigma_{3N,\pi^-} = \frac{f_{\pi^-}}{2!} R_3 \tag{11}$$

for π^+ and π^-, respectively (the factors 3! and 2! are the multiplicity of detection of the outgoing nucleons, 3 protons for π^+ and 1 proton, 2 neutrons for π^-). The errors Δf of the 12 factors f shown in the table include the statistical error and the uncertainty of the fit. The error of the average $\langle f \rangle$ is the standard deviation of f.

In addition to this error, we had the following contributions to a systematic error: 4% uncertainty in the telescope acceptance $\Delta\Omega_1$; 4% uncertainty in the bars acceptance $\Delta\Omega_2$; 2% uncertainty in the number of target particles N_{tgt}; 1% uncertainty in the pion fraction f_π of the beam; 1% uncertainty in beam counts Φ; 6% uncertainty in the neutron detection efficiency η (for π^- only). Summing these errors in quadrature results in a total systematic error of 6% for π^+ $3N$ absorption, and 9% for π^- $3N$ absorption. The systematic error in σ_{3N} is negligible compared to the standard deviation of f.

C. Two-nucleon absorption cross sections

The doubly differential $2N$ absorption cross section is given by

$$\frac{d^2\sigma}{dE_1 d\Omega_1} = \frac{N_{E_1}}{\Delta\Omega_1 \Phi f_\pi N_{\mathrm{tgt}}} \cdot \frac{1}{f_{\mathrm{bars}}}. \tag{12}$$

Here the solid angle of the bars, $\Delta\Omega_2$ [cf. Eq. (5)], is replaced by the bars acceptance factor, f_{bars}. This correction accounts for the $2N$ absorption events lost due to the bars finite dimensions. For the free $\pi^+ d \rightarrow pp$ absorption process, a peak with an angular width defined by the angular acceptance of the telescope was observed in a part of the bars area. For a quasifree process, the peak of $2N$ absorption in the bars is smeared out by the Fermi momentum of the absorbing nucleon pair, which is equal in magnitude to the momentum p_3 of the third nucleon (the *"spectator"*). At conjugate angle settings and when requiring $p_3 \leqslant 150$ MeV/c (for restriction to $2N$ absorption, as was done also in [14]), we observed a Gaussian distribution of events over the bars, both in horizontal and vertical directions, extending beyond the physical limits of the bars. Fitting a Gaussian to this distribution in both directions yielded the horizontal and vertical acceptances. Their product yielded the total bars acceptance, f_{bars}. The acceptance decreases systematically from 0.90 for the most forward bar angle to 0.83 for the most backward one. This decrease is caused by the corresponding increase in the ratio of the Fermi momentum to the momentum transferred in the absorption process to the particle going towards the bars. Because the tails of the Gaussian distribution are characterized by relatively large momenta of the third nucleon (p_3), application of this acceptance correction also corrects for the contributions to $2N$ absorption from $p_3 > 150$ MeV/c.

An example of net energy spectra of the telescope [Eq. (2)] transformed into doubly differential cross sections by Eq. (12) is shown in Figs. 6(a) and 6(b). For the $2N$ differential cross sections, background from $3N$ reactions had to be subtracted. This was done with the help of the nonconjugate angle data. For each of the six conjugate angles, the average $f \pm \Delta f$ was calculated from the two nonconjugate angular configurations adjacent to that angular setting. The phase space calculated at the conjugate angle and multiplied by the corresponding factor f was then subtracted from the $2N$ spectrum. Strictly speaking, this is wrong, as the two processes add by their amplitudes, not by their cross sections. Experimentally, this method seems to be justified, although minor interference effects cannot be fully excluded. For details see Sec. IV A. Examples for the resulting $3N$ background are shown in Fig. 6 (solid line), together with the corresponding data points at the same angles. The error Δf introduces an additional error in the $2N$ doubly differential cross section. Designating the phase space by φ, we rewrite Eq. (12) by

$$\frac{d^2\sigma}{dE_1 d\Omega_1} = \left(\frac{N_{E_1}}{\Delta\Omega_1 \Phi f_\pi N_{\mathrm{tgt}}} - f\varphi \right) \cdot \frac{1}{f_{\mathrm{bars}}}. \tag{13}$$

After subtracting the $3N$ absorption background from the doubly differential cross sections, one gets the final spectra of $d^2\sigma/(dE_1 d\Omega_1)$ versus E_1. The π^- spectrum [Fig. 6(b)] still shows three peaks. The first one (at lowest proton energy in the telescope) is due to FSI with two nucleons (the proton observed in the telescope and the undetected nucleon) recoiling together against the nucleon detected in the bars. The third peak at the high energy edge is also due to FSI. In this case, the proton detected in the telescope recoils back to back against the two nucleons going towards the bars. The peak in the center between these two FSI peaks is from $2N$ absorption, where no momentum is transferred to the third (unobserved) nucleon. Three Gaussian functions were fitted simultaneously to these peaks. The shape of the central $2N$ absorption peak was fixed by the π^+ runs and used also for π^- data taken at the same angles, where peak shape and position were essentially identical, but statistics were better for π^+. Also for π^+ the FSI peak hardly disturbed the shape of the $2N$ peak. Although the FSI peaks are much smaller for π^+ absorption, when compared to the $2N$ peak, they are clearly visible at the low energy ends of the spectra, at all angles. The high energy FSI peak is seen in π^+ absorption at backward angles, where the $2N$ peak moves to lower energies, thus separating from the FSI peak. At forward angles, the high energy FSI peak merges with the $2N$ peak.

The integral over energy of the $2N$ peak yielded the differential cross section for a given angle. The error in $2N$ absorption consists of the statistical error ΔN, the uncertainty in $3N$ background subtraction Δf, and the systematic error. The two angle-dependent errors ΔN and Δf lead to the following error in the doubly differential cross section:

$$\Delta\left(\frac{d^2\sigma}{dE_1 d\Omega_1} \right) = \frac{1}{f_{\mathrm{bars}}} \sqrt{\left(\frac{d^2\sigma}{dE_1 d\Omega_1} \cdot \frac{\Delta N_{E_1}}{N_{E_1}} \right)^2 + (\Delta f \cdot \varphi)^2}. \tag{14}$$

The systematic error consists of the components listed for the $3N$ absorption, except for the term $\Delta\Omega_2$ which is replaced by the uncertainty in f_{bars}. This uncertainty is close to 3% at all angles. The total systematic error for $2N$ absorption is therefore virtually identical to the $3N$ error (6% for π^+, 8% for π^-).

D. Final-state interaction and singles analysis

The $3N$ absorption analysis showed that a simultaneous fit of the phase space to the data over all eight bars, at angles 30° off conjugate, is impossible. This is due to a dynamical enhancement of the FSI observed in the bars near the conjugate angle. An analysis of all events for which the recoil momentum $p_3 \geqslant 200$ MeV/c (excluding $2N$ absorption, but including FSI), carried out through the conjugate angle, showed that the FSI is enhanced by a factor of up to 20 with respect to the average factor f observed at angles without FSI influence. This enhancement finds visible expression in the energy spectra of the telescopes at conjugate angles, where two FSI peaks remain on both sides of the $2N$ absorption peak, even after subtracting the phase-space normalized $3N$ background [Fig. 6(b)]. At the pion energy of the present work, the FSI influence is significant in an angular range of about 30° to both sides of the center of the FSI peak. Averaging the normalization of phase space to data over all eight bars, at angular combinations 30° off conjugate, would therefore have given a mixture of $3N$ absorption and an *unknown* fraction of the FSI. This was the reason to avoid FSI contributions in the $3N$ analysis. A correct analysis of the FSI contribution to the total cross section would demand an analysis of the peaks seen at the conjugate angles, with corrections for detector thresholds and acceptances by Monte Carlo modeling. This will not be done in this paper.

For π^-, the high energy FSI peak (HE FSI) of the coincidence runs was used to estimate the cross section contribution of these peaks. The way of calculation is exactly the

TABLE II. Differential cross sections of $2N$ π^+ absorption on ^{3}He at $T_\pi=37.0$ MeV. The errors in this table are statistical errors and background subtraction uncertainties only.

			π^+		π^-	
θ_{lab}	$\theta_{\mathrm{c.m.}}$	Jac	$d\sigma/d\Omega_{\mathrm{lab}}$ (μb/sr)	$d\sigma/d\Omega_{\mathrm{c.m.}}$ (μb/sr)	$d\sigma/d\Omega_{\mathrm{lab}}$ (μb/sr)	$d\sigma/d\Omega_{\mathrm{c.m.}}$ (μb/sr)
35.0°	39.4°	0.815	2012 ± 137	1640 ± 112	57.9 ± 5.6	47.2 ± 4.6
50.0°	55.9°	0.853	1410 ± 97	1203 ± 83	30.0 ± 4.7	25.6 ± 4.0
65.0°	71.9°	0.903	900 ± 63	813 ± 57	12.6 ± 15.2	11.4 ± 13.7
80.0°	87.5°	0.965	661 ± 50	638 ± 48	24.2 ± 4.6	23.4 ± 4.4
100.0°	107.5°	1.058	828 ± 69	876 ± 73	53.3 ± 12.4	56.4 ± 13.1
120.0°	126.5°	1.156	1226 ± 91	1417 ± 105	98.2 ± 17.5	113.5 ± 20.2

same as described above for the $2N$ absorption from the $2N$ peaks (Sec. III C). The factor f_{bars} was recalculated for the distribution of FSI events over the bars which is also of Gaussian shape. No further corrections for the bars acceptance was made (except for neutron efficiency correction). This approximation is not too bad: For the π^- HE FSI peak, two neutrons are going towards the bars. On the average, one of them is below detection threshold, one above. So for this peak, the error introduced by neglecting rigorous acceptance corrections is estimated to be $\leqslant$ 20%.

For π^+, this method of calculating the FSI cross section cannot be applied, as the HE FSI peak is not (clearly) separated from the $2N$ peak. In this case, a completely different approach made the extraction of FSI cross sections possible. Proton single-arm measurements allow an independent deduction of the $3N$ total cross section, including the FSI component. Contributions to the differential cross section of the singles runs, $(d\sigma/d\Omega)_{\mathrm{sng}}$, at this energy, are from pion absorption alone ($2N$, $3N$, and FSI). For the setup of this experiment, knock-out protons from $^3\mathrm{He}(\pi^\pm,\pi^\pm p)pn$ reach a maximum energy of 12 MeV at $\theta_{\mathrm{TEL}}=35°$, which is below the detection threshold of the telescopes (26 MeV).

The yield for singles runs is given by

$$N=N_1-K(N_3), \tag{15}$$

with N_1 the total number of events with the full target, N_3 the total number of events with the empty target, and K the beam counts normalization factor as defined above. The statistical error is given by

$$\Delta\left(\frac{d^2\sigma}{dE_1 d\Omega_1}\right)=\frac{d^2\sigma}{dE_1 d\Omega_1}\cdot\frac{\Delta N_{E_1}}{N_{E_1}}, \tag{16}$$

with ΔN composed of the errors in N_1 and N_3 only.

The starting point for our calculation of $\sigma_{\mathrm{FSI}\pi^+}$ is the decomposition of the differential cross section of singles events for π^+, $(d\sigma/d\Omega)_{\mathrm{sng}}$:

$$\left(\frac{d\sigma}{d\Omega}\right)_{\mathrm{sng}}=2\left(\frac{d\sigma}{d\Omega}\right)_{2N}+\frac{3}{C}\left(\frac{d\sigma}{d\Omega}\right)_{3N}+\frac{3}{D}\left(\frac{d\sigma}{d\Omega}\right)_{\mathrm{FSI}}. \tag{17}$$

The numerical factors are the multiplicities of protons detected in the telescope for each process. The first term on the right-hand side is the $2N$ absorption differential cross section actually measured (Table II). The second term is a differential $3N$ absorption cross section, but actually only the integrated value σ_{3N} is measured in the experiment. $(d\sigma/d\Omega)_{3N}$ is multiplied by a factor C that corrects for the energy threshold of the telescopes. This factor is the ratio of phase space without and with the energy threshold. It varies between 1.14 and 1.20 for telescope angles between 35° and 120°. Similarly, the factor D corrects for the energy threshold for detecting the two protons in the FSI LE peak. This factor is somewhat larger than C and is estimated to be 1.5 $\pm$ 0.2. This yields an expression for the $3N$ differential cross sections, $(d\sigma/d\Omega)_{3N}$:

$$3(d\sigma/d\Omega)_{3N}=C\left[(d\sigma/d\Omega)_{\mathrm{sng}}-2(d\sigma/d\Omega)_{2N}-2\left(\frac{d\sigma}{d\Omega}\right)_{\mathrm{FSI}}\right]. \tag{18}$$

At the angles measured, we calculate $(d\sigma/d\Omega)_{\mathrm{mix}}\equiv C\cdot[(d\sigma/d\Omega)_{\mathrm{sng}}-2(d\sigma/d\Omega)_{2N}]$ (see Table V and Fig. 12). Integration over all angles yields

$$\sigma_{\mathrm{mix}}=3\sigma_{3N}+C\cdot 2\sigma_{\mathrm{FSI}} \tag{19}$$

(called σ_{mix} as it contains a mixture of $3N$ and FSI cross sections). Finally, we solve for σ_{FSI} to get

$$\sigma_{\mathrm{FSI}}=\frac{\sigma_{\mathrm{mix}}-3\sigma_{3N}}{1.17\cdot 2}, \tag{20}$$

where we used the average value of 1.17 for the factor C. In the present experiment, this technique could not be applied to π^- absorption due to various technical problems with the π^- single-arm measurements. The total systematic error for singles is slightly less than for the coincidence runs (Sec. III B) as the uncertainty factor of the bars drops out. It amounts to 5% for the π^+ beam.

IV. RESULTS

A. Spectator momentum distribution

The momentum distribution of the spectator nucleon can determine to what extent the $2N$ absorption is a quasifree process. It is given by

$$\rho_{p_3}=\left(\frac{d^2\sigma}{d\Omega_1 dp_3}\right)\left(p_3^2 dp_3\int_R dR\right). \tag{21}$$

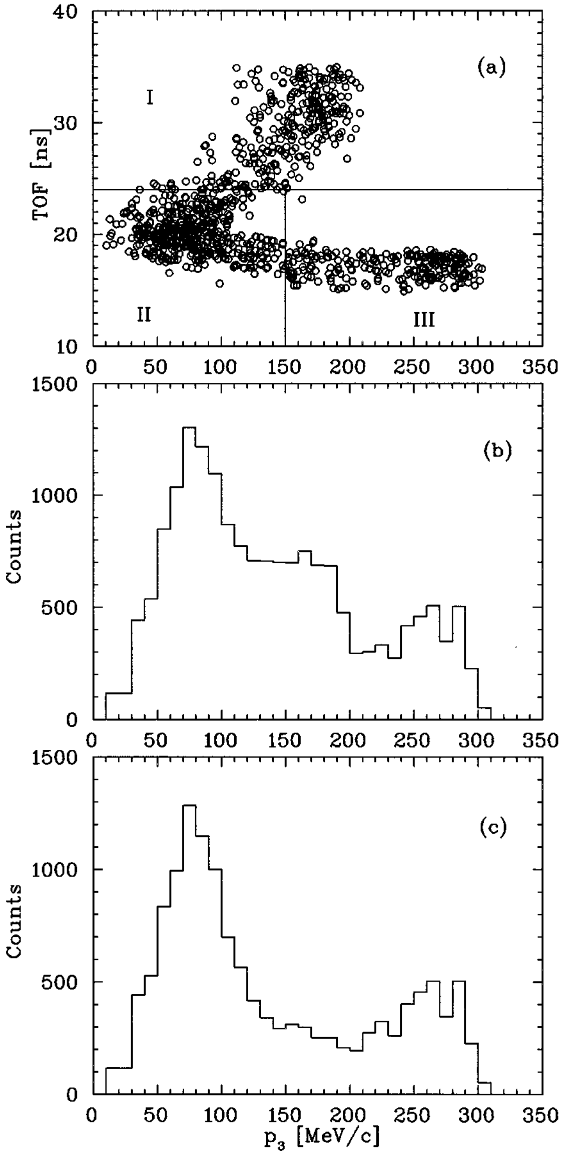

FIG. 8. Spectator momentum distribution (π^-, $\theta_{\mathrm{TEL}}=35°$, $\theta_{\mathrm{bars}}=135°$). (a) TOF of the neutrons detected in the bars vs the calculated spectator momenta, showing different kinematic regions: region II is the $2N$ absorption region, I and III are both dominated by FSI. (b) Projection of (a) on the p_3 axis. The peaks of the three regions are overlapping. (c) Same as (b), but after cut excluding region I. The $2N$ peak is now cleaner, but still contaminated by the tail of the FSI peak of region I.

Here, $d^2\sigma/d\Omega_1 dp_3$ is measured in the experiment, and $p_3^2 dp_3 \int_R dR$ is the three-nucleon phase space, integrated over all variables except for p_3, and corrected for the experimental acceptances. The detailed description of this equation is given in [14,32]. We calculated the phase space with the experimental configurations using a Monte Carlo program. The resulting momentum distributions are shown in Fig. 7. They are compared to the results of the momentum distribution measurements (solid and dashed lines in Fig. 7) for a proton in ^{3}He, based on the ^{3}He$(e,e'p)$ study by Jans *et al.* [22,23]. One expects the proton and neutron momentum distributions in ^{3}He to be similar.

The open circles in Fig. 7 show the momentum distribution obtained for π^+ (a) and π^- (b), with the data of the three telescopes added together. The angular configuration chosen has the bars at 135°; one telescope at the conjugate angle (35°), one at 65°, and one at 95°. The momentum region $p_3 \geqslant 320$ MeV/c corresponds to the angular region farthest from the conjugate angle. The $3N$ absorption analysis showed that this is the only region without any FSI contributions. After calculating the $3N$ absorption phase space over the whole region, a least squares fit was made for the

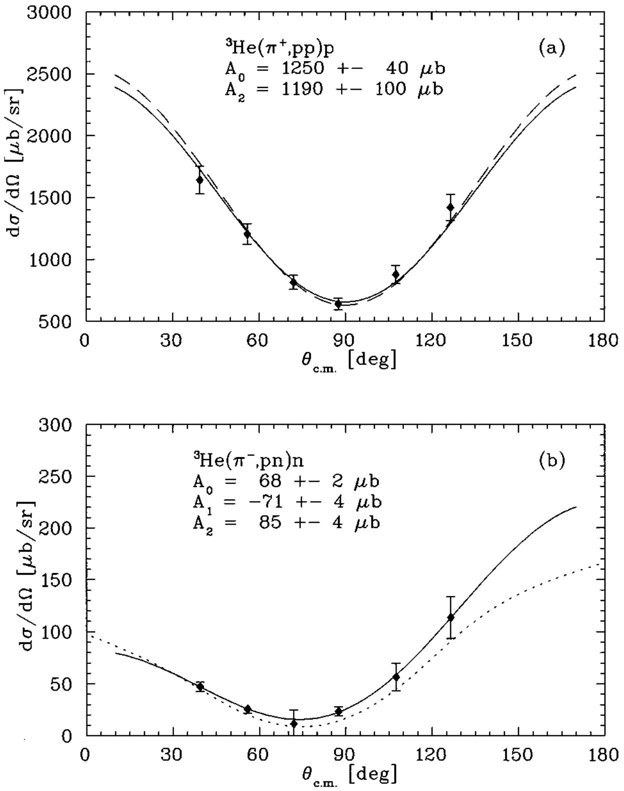

FIG. 9. Angular distribution of the $2N$ π^+ absorption (a) and the $2N$ π^- absorption (b) on ^{3}He at $T_\pi=37.0$ MeV. The solid lines are the Legendre polynomial fits to the data. The dashed line in (a) is the angular distribution of $\pi^+(d,pp)$ at 40 MeV [26], scaled by the factor 1.5. The dotted line in (b) is the theoretical result of Niskanen [43].

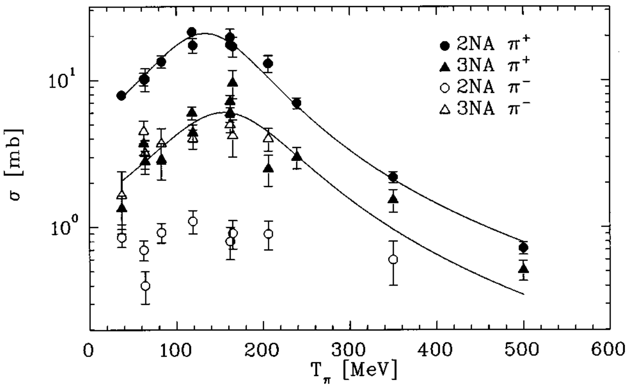

FIG. 10. Results of π^+ and π^- $2N$ and $3N$ absorption measurements on ^{3}He at different pion energies. For details, see Table IX. The lines are a Lorentz fit to the π^+ data.

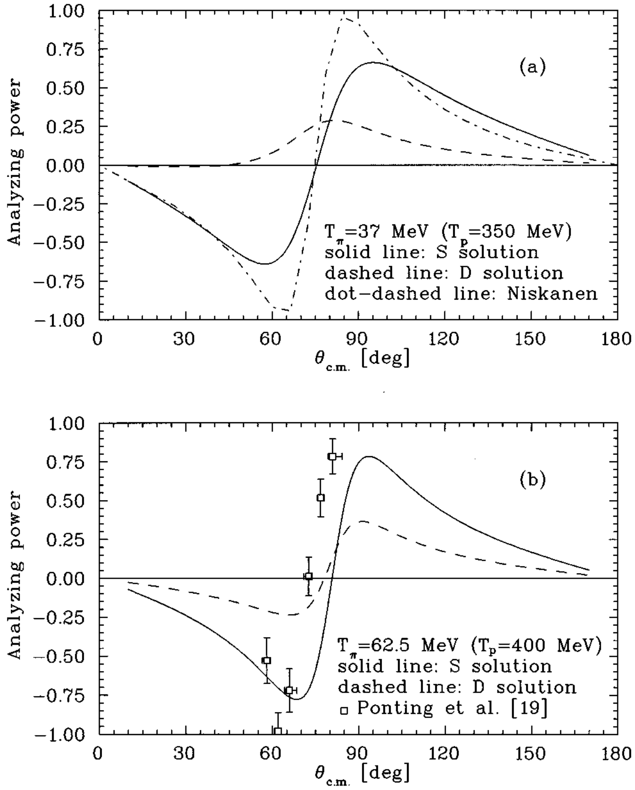

FIG. 11. The two solutions for polarization as predicted by partial wave amplitude analysis of the pion absorption experiments for $T_\pi = 37.0$ and 62.5 MeV. For both energies, the dashed line shows the asymmetry predicted by the "*D*" solution giving more weight to the $^3D_1$ channel; the solid line shows the asymmetry predicted by the "*S*" solution giving more weight to the $^3S_1$ channel. The predictions are based on the $2N$ π^- absorption results of the present work for 37.0 MeV, of Aniol *et al.* [13] for 62.5 MeV, and updated *pn* elastic scattering phase shifts [34]. Included are the theoretical prediction of Niskanen [43] for 37.0 MeV, and the data of Ponting *et al.* [19] for $T_p = 400$ MeV.

region $p_3 \geqslant 320$ MeV/c. The normalization factors obtained in this way were $f = 0.096 \pm 0.012$ for π^+, and $f = 0.041 \pm 0.006$ for π^-, consistent with those obtained in the $3N$ analysis (the last two lines of Table III). The phase space was then multiplied by this factor and subtracted from the data over the whole region. The momentum distribution after this subtraction is shown by the solid circles in Fig. 7. For the region above 320 MeV/c, where there are virtually no $2N$ and FSI contributions, the distribution approaches zero. At lower recoil momenta, the $3N$ background subtraction hardly makes a difference, due to the large FSI and $2N$ absorption cross sections there.

Lacking an analytic way to subtract the FSI, an attempt was made to subtract it at least partially. To understand the procedure, it is useful to look at the scatter plot of TOF versus p_3 [Fig. 8(a)] for the same experimental conditions as in Fig. 7(b) (π^-). Three kinematical regions can be separated: Region II is the $2N$ absorption region (p_3 around the *rms* value of Fermi momentum in ^{3}He). Region III is mainly due to FSI, with a *pn* pair recoiling against a single neutron. Region I is also due to FSI. Here, an *nn* pair is recoiling against a single proton which is recorded in the telescope with high energy [Fig. 6(b)].

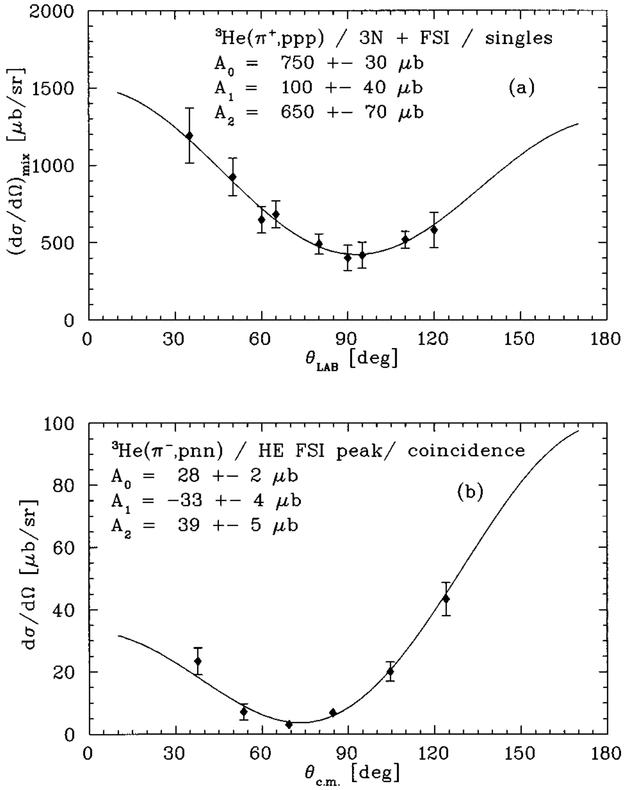

FIG. 12. FSI angular distributions. (a) The "mixed" results $(d\sigma/d\Omega)_{\text{mix}} \equiv C \cdot [(d\sigma/d\Omega)_{\text{sng}} - 2(d\sigma/d\Omega)_{2N}]$ from π^+ singles. A pure $3N$ phase-space-like behavior would result in a flat distribution. The difference in shape is due to the FSI contribution. Lab angles are used as there is no unique c.m. system for the plotted quantities. (b) $(d\sigma/d\Omega)_{\text{FSI}}$ from the π^- HE FSI peaks. The distribution has a shape similar to that of π^- $2N$ absorption, in contrast to pure $3N$ phase space.

Figure 8(b) shows a projection on the p_3 axis of the scatterplot Fig. 8(a). It can be seen that the three peaks cannot be separated when looking at the spectrum of the recoil momentum alone. In Fig. 8(c), region I was removed from the scatterplot, before making the projection. Now, the $2N$ peak appears more clearly separated. The crosses in Fig. 7 represent the momentum distribution after subtracting, in addition to the $3N$ phase space, this FSI peak [region I of Fig. 8(a)]. This was done for the conjugate angle only; thus, FSI measured in the telescope at the 30° off-conjugate angle remain, contributing to the momentum region between ≈ 150 and ≈ 200 MeV/c. The FSI of region III (200 MeV/$c \leqslant p_3 \leqslant 300$ MeV/c) which was not subtracted causes the two curves (solid circles and crosses) to coincide in the momentum region above ≈ 200 MeV/c.

For π^+ [Fig. 7(a)], where the FSI cross section is small as compared to the $2N$ absorption cross section, the result shows satisfying agreement with the measurement of Jans *et al.* in the $2N$ region (up to 150 MeV/c). The deviations between 60 and 110 MeV/c may be (at least partly) explained by a remaining tail of the FSI peak of region I. The influence of the remaining tail of the FSI peak, in this momentum region, is even more evident in the momentum distribution of π^-.

Note that the cut made in Fig. 8(a) to separate region I

TABLE III. Results for three-body absorption at $T_\pi = 37.0$ MeV. The "angular distance" is the distance (in degrees) from the two-body absorption peak.

θ_{TEL}	θ_{bar}	Range of the bars	Angular Distance	f_{π^+}	f_{π^-}
90.0°	39.2°	10.7°	35.7°	0.108 ± 0.016	0.082 ± 0.015
60.0°	48.0°	28.6°	57.9°	0.128 ± 0.010	0.042 ± 0.012
70.0°	57.2°	10.7°	37.9°	0.079 ± 0.023	0.064 ± 0.010
40.0°	66.0°	28.6°	63.1°	0.106 ± 0.017	0.037 ± 0.011
110.0°	93.8°	10.7°	37.4°	0.094 ± 0.006	0.036 ± 0.006
50.0°	76.2°	10.7°	41.1°	0.091 ± 0.008	0.039 ± 0.012
95.0°	109.8°	10.7°	39.7°	0.077 ± 0.006	0.023 ± 0.010
35.0°	92.2°	10.7°	43.0°	0.124 ± 0.009	0.059 ± 0.019
110.0°	118.0°	28.6°	61.6°	0.064 ± 0.006	0.031 ± 0.009
80.0°	126.8°	10.7°	42.1°	0.115 ± 0.009	0.034 ± 0.012
95.0°	135.0°	28.6°	64.9°	0.073 ± 0.008	0.028 ± 0.013
65.0°	143.8°	10.7°	43.4°	0.127 ± 0.011	0.024 ± 0.016
			$\langle f \rangle$	0.092 ± 0.024	0.039 ± 0.018
			σ_{3N}	1.25 ± 0.32 mb	1.55 ± 0.72 mb

from region II is rather arbitrary. The $2N$ absorption and the FSI regions overlap here. No analytic separation of the two regions is possible. Because of this uncertainty in FSI subtraction and because of the relative strength of the FSI (especially for π^-), the $2N$ absorption analysis of the present work was not based on the recoil momentum distribution. Instead, the energy spectra of the telescopes were used. They allow a good separation of the different peaks. The recoil spectra such as the one shown in Fig. 8(c) were used as a crosscheck. After the cut on FSI region I in the scatterplot, a Gaussian fit to the $2N$ peak minimized the influence of the remaining FSI tail underlying the high momentum end of the $2N$ peak. The two methods gave consistent results for the differential $2N$ absorption cross sections.

The spectator momentum distribution also justifies to a certain extent the method of removing $3N$ background by subtracting $3N$ from $2N$ cross sections, disregarding possible interference effects. At pion energies of 350 and 500 MeV, FSI was not disturbing the momentum distribution. At these energies a simultaneous fit to the $2N$ region (based on the known momentum distribution as given by the solid line in Fig. 7) and to the $3N$ region (based on phase space) accounted for all the observed events, without any obvious interference effects (Smith *et al.* [32]). At 37.0 MeV, FSI contaminates the region where interference effects should most easily be noticed (150 MeV/$c < p_3 < 200$ MeV/c). From the energy distribution in the telescopes, these events are identified as belonging to the FSI peaks, not to the $2N$ absorption peak. The situation is not as clear as at 350 and 500 MeV, and interference effects cannot be fully excluded. But after separating $2N$, $3N$, and FSI, remaining interference effects can be only small as compared to these three components. In addition, the ratio of absorption cross sections between π^{+3}He and $\pi^+ d$ is observed to be consistent with the number of np pairs at 37.0 MeV (see below Sec. V A 1 and [30]). The combination of these two observations makes it plausible to treat, as a practical approach, the $2N$ and $3N$ amplitudes incoherently.

B. Two-nucleon absorption

1. π^+ absorption on a (pn) pair

The differential cross sections are obtained as described in Sec. III. The results are listed in Table II and shown in Fig. 9. The solid line is a fit to the data by a Legendre polynomial expansion of order 2:

$$d\sigma/d\Omega = A_0 + A_2 P_2(\cos\theta). \tag{22}$$

The asymmetry term $P_1(\cos\theta)$ vanishes because of the intrinsic symmetry of the distribution of two identical particles in the final state. We assume that at $T_\pi = 37.0$ MeV only s- and p-wave pions contribute to the process, and therefore neglect higher order terms in the polynomial expansion. The results $A_0 = 1250 \pm 40$ μb, $A_2 = 1190 \pm 100$ μb.

The angle-integrated cross section $\sigma_{2N\pi^+}$ is given by $4\pi A_0$, divided by 2 (two identical particles in the final state):

$$\sigma_{2N\pi^+} = 2\pi A_0 = 7.9 \pm 0.5 \text{ mb}. \tag{23}$$

The error includes a systematic error of 6%.

2. π^- absorption on a diproton

The differential cross sections are obtained as described in Sec. III. Results are in Table II and Fig. 9. The solid line is a fit to the data by a Legendre polynomial expansion of order 2:

$$d\sigma/d\Omega = A_0 + A_1 P_1(\cos\theta) + A_2 P_2(\cos\theta). \tag{24}$$

The results $A_0 = 68 \pm 2$ μb, $A_1 = -71 \pm 4$ μb, $A_2 = 85 \pm 4$ μb.

The total cross section is

$$\sigma_{2N\pi^-} = 4\pi A_0 = 0.85 \pm 0.08 \text{ mb}. \tag{25}$$

The main contribution to the error is from the systematic error of 8% (cf. end of Sec. III).

C. Three-nucleon absorption

The results of the $3N$ absorption, calculated as described in Sec. III B, are summarized in Table III. The reduced χ^2 of the fit of phase space to data at the 12 angular combinations varies between 0.9 and 2.5 for π^+ and between 0.4 and 1.5 for π^-. This indicates that the assumption that $3N$ absorption behaves like a phase space at the individual angular combinations is reasonable.

The error for the weighted average $\langle f \rangle$ shown in the table is the error from the standard deviation in f. The weighted average error of f is much smaller (π^+: 0.0024, π^-: 0.0031). The large differences between the standard deviations and the weighted average errors indicate that our assumption of a constant factor f is reasonable over limited regions of the phase space but does not hold over the whole phase space. Lacking other possibilities to calculate σ_{3N}, we use the averaged $\langle f \rangle$, which still should be close to reality as no extreme deviations in f are observed.

TABLE IV. Results for three-body absorption at $T_\pi = 62.5$ and 82.8 MeV.

62.5 MeV				82.8 MeV			
θ_{TEL}	θ_{bar}	f_{π^+}	f_{π^-}	θ_{TEL}	θ_{bar}	f_{π^+}	f_{π^-}
65.0°	133.0°	0.20±0.04		65.0°	129.9°	0.14±0.01	0.06±0.01
				95.0°	129.9°	0.11±0.04	0.06±0.01
80.0°	114.0°	0.18±0.02		80.0°	110.8°	0.16±0.03	0.05±0.01
				110.0°	110.8°	0.08±0.02	0.05±0.01
35.0°	97.0°	0.25±0.03					
95.0°	97.0°	0.21±0.02					
50.0°	81.0°	0.20±0.04		50.0°	77.8°		0.04±0.01
				110.0°	77.8°		0.07±0.01
40.0°	62.0°	0.17±0.03		40.0°	59.2°	0.14±0.02	0.06±0.02
70.0°	62.0°	0.19±0.03		70.0°	59.2°		0.05±0.01
				60.0°	42.6°	0.18±0.06	0.06±0.02
90.0°	45.0°	0.27±0.04		90.0°	42.6°		0.10±0.02
	$\langle f \rangle$	0.21±0.04	0.09±0.02		$\langle f \rangle$	0.13±0.04	0.06±0.02
	σ_{3N}	3.7±0.6 mb	4.5±0.8 mb		σ_{3N}	2.8±0.8 mb	3.4±1.1 mb

D. Three-nucleon absorption at T_π = 62.5 and 82.8 MeV

The $3N$ absorption data of Aniol *et al.* [13] were reanalyzed in a way similar to the procedure described in Sec. III B, where Eq. (7) replaces the incorrect equation in Table II of [13]. The factors f resulting from the fit and the total $3N$ cross sections are listed in Table IV. For π^- at 62.5 MeV, raw data were no longer available. In this case, the average factor $\langle f \rangle$ was extrapolated from the average ratio of the new factor $\langle f \rangle$ to the one given in [13], at $T_\pi = 82.8$ MeV (π^+ and π^-), and $T_\pi = 62.5$ MeV (π^+). This ratio is 0.5–0.6 in all three cases. Consequently, the resulting $3N$ total cross sections are smaller by the same factor as those cited in the work of Aniol *et al.* [13]. One of these four $3N$ cross sections ($T_\pi = 62.5$ MeV, π^+) was calculated in the work of Aniol independently, based on singles runs, resulting in $\sigma_{3N} = 3.6 \pm 0.4$ mb. This value agrees with the one calculated in the present reanalysis ($\sigma_{3N} = 3.7 \pm 0.6$ mb).

TABLE V. $(d\sigma/d\Omega)_{\mathrm{mix}} \equiv C \cdot [(d\sigma/d\Omega)_{\mathrm{sng}} - 2(d\sigma/d\Omega)_{2N}]$ for π^+ (from singles runs), and the differential cross sections $(d\sigma/d\Omega)_{\mathrm{FSI,HE}}$ of the FSI peak at the high energy edge from π^- coincidence runs.

	π^+		π^-	
θ_{TEL}	$(d\sigma/d\Omega)_{\mathrm{mix}}$ (lab) (μb/sr)	$(d\sigma/d\Omega)_{\mathrm{FSI,HE}}$ (lab) (μb/sr)	$\theta_{\mathrm{c.m.}}$	$(d\sigma/d\Omega)_{\mathrm{FSI,HE}}$ (c.m.) (μb/sr)
35°	1191±177	26.6±4.9	37.7°	23.4±4.3
50°	924±120	7.9±2.9	53.6°	7.1±2.6
60°	647±86			
65°	682±88	3.3±1.4	69.3°	3.1±1.3
80°	490±65	7.0±1.3	84.6°	6.8±1.2
90°	400±81			
95°	417±84			
100°		19.4±3.0	104.6°	20.0±3.1
110°	518±55			
120°	581±114	39.8±4.9	124.0°	43.4±5.3

E. Final-state interaction

As explained in Sec. III D, the FSI cross sections for π^+ and π^- absorption were calculated in different ways. For π^+, a mixed (lab) differential cross section $(d\sigma/d\Omega)_{\mathrm{mix}} \equiv C \cdot [(d\sigma/d\Omega)_{\mathrm{sng}} - (d\sigma/d\Omega)_{2N}]$ was extracted from singles runs. For π^-, the c.m. differential cross sections of the FSI peak at the high energy edge of the proton spectrum in the telescope were calculated from coincidence runs. The resulting differential cross sections are listed in Table V and shown in Fig. 12.

Legendre polynomial fits to the two distributions yielded the coefficients listed in Table VI. The total cross section for the π^- HE FSI peak was calculated directly from A_0:

$$\sigma_{\mathrm{FSI,HE}}(\pi^-) = 4\pi A_0 = 0.35 \pm 0.03 \pm 0.07 \text{ mb}. \tag{26}$$

The first error is from the fit only; the second one takes into account the uncertainty of $\leqslant 20\%$ due to acceptance problems, and the systematic error of 5%. For the total π^- FSI absorption, the yield of the low energy FSI peak has to be added. It is not necessarily identical to the HE FSI yield, as the two nucleons pairing off are different. But it can be expected to be similar. The total FSI π^- cross section is therefore estimated to be 0.7 ± 0.2 mb.

For π^+, the integration over the angular range gives $4\pi A_0 = 9.4 \pm 0.6$ mb (error including systematic error) which is σ_{mix} as defined in Eq. (19). σ_{FSI} is then calculated from σ_{mix} and σ_{3N}, using Eq. (20). The result $\sigma_{\mathrm{FSI}}(\pi^+) = 2.4 \pm 0.7$ mb.

TABLE VI. Legendre polynomial coefficients for $(d\sigma/d\Omega)_{\mathrm{mix}}$ (π^+) and $(d\sigma/d\Omega)_{\mathrm{FSI,HE}}$ (π^-).

	A_0 μb	A_1 μb	A_2 μb	χ^2/ν
π^+	749±26	103±42	648±72	0.48
π^-	28±2	−33±4	39±5	1.0

TABLE VII. Cross sections and Legendre polynomial ratios of π^+ and π^- $2N$ absorption. Errors include statistical and systematic uncertainties. The column $\theta_{\mathrm{c.m.(min)}}$ shows the c.m. angles at which the minimum of the Legendre polynomial fit for π^- absorption is found. The value of $\theta_{\min}$ cited for 165 MeV is from a fit including A_3 (Mukhopadhyay [17]). p.w. stands for "present work."

T_π (MeV)	$\sigma_{2N\pi^+}$ mb	A_2/A_0	$\sigma_{2N\pi^-}$ mb	A_1/A_0	A_2/A_0	$\theta_{\mathrm{c.m.(min)}}$ deg
37.0 [p.w.]	7.9±0.5	0.95±0.09	0.85±0.08	−1.04±0.07	1.3±0.1	74±1
62.5 [13]	10.2±1.0	1.14±0.11	0.70±0.11	−0.82±0.13	1.6±0.2	80±2
64 [14,15]	10.2±1.8	1.17±0.06	0.4±0.1	−0.90±0.05	1.4±0.1	78±1
82.8 [13]	13.4±1.3	1.10±0.07	0.92±0.14	−0.79±0.13	1.7±0.2	81±2
119 [14,15]	17.3±2.0	1.10±0.06	1.1±0.2	−0.77±0.15	1.7±0.1	81±2
162 [14,15]	19.6±2.7	1.17±0.10	0.8±0.2	−0.69±0.05	1.9±0.1	83±1
165 [17]	17.0±2.6	1.01±0.09	0.91±0.20	−0.76±0.14	1.4±0.2	87±2
206 [14,15]	13.0±1.7	1.33±0.10	0.9±0.2	−0.19±0.07	1.6±0.1	88±1
350 [32]	2.19±0.19	0.86±0.08	0.6±0.2[16]			
500 [32]	0.72±0.07	0.44±0.06				

V. DISCUSSION

A. Two-nucleon absorption

1. π^+ absorption on a (pn) pair

The ratio of the Legendre polynomial coefficients A_2/A_0 (0.95±0.09) is close to unity as found at higher energies (Table VII). This value is consistent with the value of A_2/A_0 measured in π^+ absorption on the deuteron (1.01 at both 35 and 40 MeV [26]). It is expected to be unity as long as the p partial wave leading to the $^1D_2$ final NN state is dominant [33]. The slightly smaller value measured at 37.0 MeV is in agreement with the trend for the deuterons at low energies, indicating an increasing contribution from s-wave absorption.

The total cross section is a factor of 1.5±0.15 times the cross sections measured for $d(\pi^+,pp)$ at $T_\pi = 35$ and 40 MeV [26], as expected from counting 1.5 pn pairs with the deuteron quantum numbers in ^{3}He. This and the factor of ≈ 10 between the π^+ and π^- cross sections indicate that even at this low energy the channel with an intermediate ΔN is dominating other effects such as the higher density.

2. π^- absorption on a diproton

The angular distribution of the differential cross sections is backward peaked (Fig. 9) as has been observed at all energies at which π^- absorption on ^{3}He has thus far been measured. The Legendre polynomial coefficients reported for the different experiments, assuming only s- and p-wave pion contributions, are listed in Table VII. The ratio A_2/A_0 is rather stable over the whole energy range, especially when averaging the two values reported for 162 and 165 MeV, yet slightly decreasing at low energies as for π^+ absorption. The ratio $|A_1/A_0|$ is a measure of the asymmetry of the distribution. After averaging the values at 162 and 165 MeV, the general tendency is an increase in the asymmetry with decreasing beam energy, also reflected in smaller values of $\theta_{\min}$. These are indications of increasing contributions from s-wave, and of s- and p-wave interference, with decreasing energy.

The angle integrated cross sections are listed in Table VII and Fig. 10. The energy dependence of the cross sections (Fig. 10) does not show any effect of the Δ resonance. Except for the point at 64 MeV, the distribution looks fairly flat. The average of all values is 0.8±0.2 mb.

With the assumption that only s- and p-wave pions contribute at low energies, the number of transition amplitudes is restricted to three, leading to three final pn states: for $l_\pi=0$, final pn = $^3P_0$; for $l_\pi=1$, final pn = $^3S_1$, or $^3D_1$. In the following the three amplitudes will be referred to by their final pn states. Piasetzky *et al.* [18] studied the relation between the transition amplitudes for the three channels, and the coefficients of the Legendre polynomial fit to the differential cross sections of π^- absorption on the diproton. For the results of Aniol *et al.* [13] at $T_\pi=62.5$ MeV they found two possible amplitude solutions, both in agreement with the data. The solutions differ significantly in the relative strengths of the $^3S_1$ and $^3D_1$ amplitudes, and are therefore called the "*S*" and "*D*" solution according to the dominant amplitude. Furthermore, they showed that the two solutions lead to a different angular dependence of the polarization of the final state proton.

The analysis procedure as described by Piasetzky *et al.* employs Watson's theorem allowing the use of pn elastic-scattering phase shifts and mixing parameters to determine the phases of the three amplitudes [18]. In the present work, this procedure was applied to $T_\pi=37.0$ MeV ($T_p=350$ MeV) and repeated for $T_\pi=62.5$ MeV ($T_p=400$ MeV) using the SP93 phase shifts of Arndt [34]. The resulting predictions are shown in Fig. 11 and Table VIII. The inclusion of d waves could lead to small changes in the results we present. The polarization was measured in experiments at

TABLE VIII. Relative strength of the three transition amplitudes contributing to $\pi^- pp(^1S_0)\rightarrow pn$, for $l_\pi \leqslant 1$, based on the results of the pion absorption experiments.

Pion wave	(pn) state	$T_\pi=37.0$ MeV "*S*"	"*D*"	$T_\pi=62.5$ MeV "*S*"	"*D*"
$l_\pi=0$	$^3P_0$	0.13	0.13	0.07	0.07
$l_\pi=1$	$^3S_1$	0.59	0.27	0.52	0.09
	$^3D_1$	0.28	0.60	0.41	0.84

TRIUMF, using the inverse reaction $d(\vec{p},\pi^- pp)p$ at proton bombarding energies of $T_p=350$, 400, and 440 MeV, corresponding to pion energies of $T_\pi=37$, 65, and 85 MeV, respectively [19–21]. Previous results at $T_p=400$ MeV [19] are presented in the figure, and show that the "S" solution is in much better agreement with the experiment than the "D" solution.

The theoretical model of Maxwell and Cheung [35] for π^- absorption on the diproton, based on one boson exchange, resulted in wrong asymmetry (forward peaked). Miller and Gal [36], using a six-quark bag model, succeeded in producing the correct forward-backward asymmetry. An attempt to deduce the polarization behavior from a simple model based effectively on one-pion exchange showed modest agreement with the angular distribution, but did not reproduce the zero shift and the rather dramatic behavior of the polarization close to the zero crossing (Bachman, Riley, and Hollas [37], following the model of [38]). Models based on pion exchange alone tend to exaggerate the strength of the $^3D_1$ transition amplitude while the six-quark bag model [36] gives too large a $^3S_1$ transition amplitude. No attempt has been made so far to combine the two models.

By introducing a Galilean-invariant πNN coupling operator in a model on the hadron level, Niskanen [39] succeeded to reproduce the asymmetry observed at 62.5 MeV satisfactorily. He included d- and f-wave pions in his calculations which contributed non-negligible amplitudes, but did not effectively influence the angular distribution, thus partly justifying the neglect of these partial waves. The polarization predicted by this model resembles the data [19–21] qualitatively and is similar to the "S" solution of Fig. 11. The model is less successful in reproducing the observed asymmetry at higher energies and in predicting the total cross section, which is too high by a factor of 3–5 at 62.5 MeV (similar disagreement at 37.0 MeV).

In a recent experiment, the total cross sections near threshold for $pp\rightarrow pp\pi^\circ$ were found to be five times larger than predicted by theory [40]. In this reaction near threshold, only the $T=1$, $l_\pi=0$ channel contributes. This channel has the same quantum numbers as the $^3P_0$ (final state pn) channel for π^- absorption on the diproton (s-wave pion). To explain the unexpected enhancement of this channel, a heavy meson exchange (HME) via a nucleon-antinucleon vertex was proposed (Lee and Riska [41]; Horowitz, Meyer, and Griegel [9]). Niskanen [42] studied the impact of the HME on π^- absorption on the diproton by incorporating the meson exchange current effect into his previous [39] formalism. Inclusion of this effect which gives more weight to the s-wave pion channel results in a larger asymmetry of the angular distribution and in a shift of the zero crossing of the polarization curve to more forward angles. A second change made in [42] to adjust the strength of this channel was to replace the two-nucleon S-wave correlation function in ^{3}He calculated from the Reid soft core potential by a parametrization of the Hajduk wave function of ^{3}He (details and references in [39,42]). Inclusion of the HME current and application of the Hajduk wave function gave good agreement with the experimental data at 62.5 MeV [42] without applying any scaling factor. The results for 37.0 MeV [43] are shown together with the data in Fig. 9. Again, no scaling factor for the theoretical absorption was used. In conclusion, the present results of pion absorption at low energies, together with the analyzing power measurements at corresponding proton energies, present a useful set of data for testing the strength of the s-wave pion channel, short range effects like HME and structure of the wave function at short distances, and the ratio of $^3S_1/^3D_1$ p-wave pion channels, i.e., the strength of the tensor force or the mixing parameter ϵ_1.

B. Three-nucleon absorption

As seen in Table III, the normalization factors f do not vary much and not in any systematic way over the measured angles (Sec. IV C) meaning that the $3N$ absorption process behaves approximately like phase-space distribution. In contrast to $2N$ absorption, the total $3N$ cross sections are similar for π^+ and π^-. This similarity was also observed at higher energies (Table IX). A comparison between the results at different energies is problematic. In part of the experiments (Weber *et al.* [15] and present work), the FSI was separated from the $3N$ absorption. The results of Aniol *et al.* at 62.5 MeV, even with the corrected phase-space formula (see Sec. IV D), are larger than those of Weber *et al.* [15] at 64 MeV, and this may be caused by residual FSI influences. Compared to the results of Weber *et al.* [15], our results at 37.0 MeV show a considerable drop in the cross section. An experiment with stopped pions [24] showed that the $3N$ phase space is virtually empty; only collinear events ($2N$ and FSI) could be observed. Our result at 37.0 MeV is consistent with a drop in $3N$ absorption strength at lower energies. The cross section for FSI increases at low energies, and at 37.0 MeV becomes comparable to that of $3N$ absorption. The energy dependence of the results shows a weak Δ resonance shape (Table IX and Fig. 10). The error-weighted average of the two results at 162 and 165 MeV is 6.4 ± 0.6 mb.

For π^+, the ratio $\sigma_{3N}/(\sigma_{2N}+\sigma_{3N})$ is rather stable (20–30%) in the energy range 62.5–165 MeV. At 37.0 MeV the ratio drops to 14%. The decrease of the $2N$ cross section follows the Δ resonance, as seen by comparison with $d(\pi^+,pp)$ cross sections. The drop in the ratio shows that the $3N$ cross section decreases more rapidly than the Δ resonance. In contrast to low energies, at energies above the Δ resonance (350 and 500 MeV) the $2N$ cross section decreases more rapidly than the $3N$ cross section, causing an increase in the ratio $\sigma_{3N}/(\sigma_{2N}+\sigma_{3N})$ to 45%. For π^-, the ratio shows a similar trend but with larger values than for π^+, due to the small (π^-,pn) reaction cross section. If one assumes $\sigma(\pi^-,2n)\approx\sigma(\pi^+,2p)$ the values become comparable. The drop in the ratio at 37.0 MeV for both π^+ and π^- is a consequence of the fact that at this low energy the $3N$ phase space starts to thin out.

The $3N$ absorption processes can be roughly divided into two categories: $2N$ absorption accompanied by an interaction with the third nucleon, and genuine $3N$ absorption. The first category can be subdivided into an initial-state interaction (ISI), hard final-state interaction (HFSI), and soft final-state interaction (FSI). The latter process will be discussed in Sec. V C. For the ISI, the incident pion interacts with one of the nucleons by scattering or charge exchange, and is afterwards absorbed by the other two nucleons. It has been shown [44] that this process should have a clear experimental sig-

TABLE IX. Summary of π^+ and π^- $2N$ and $3N$ absorption cross sections. For all results, errors include statistical and systematic uncertainties. p.w. stands for "present work." The two values for $3N$ π^+ absorption at 350 and at 500 MeV are from two different methods of calculating σ_{3N}, as explained in [32] .

	π^+			π^-		
T_π (MeV)	σ_{2N} (mb)	σ_{3N} (mb)	$\frac{\sigma_{3N}}{\sigma_{2N}+\sigma_{3N}}$	σ_{2N} (mb)	σ_{3N} (mb)	$\frac{\sigma_{3N}}{\sigma_{2N}+\sigma_{3N}}$
37.0 [p.w.]	7.9±0.5	1.3±0.3	0.14±0.04	0.85±0.08	1.6±0.7	0.65±0.12
62.5 [13, p.w.]	10.2±1.0	3.7±0.6	0.27±0.05	0.70±0.11	4.5±0.8	0.87±0.04
64 [14,15]	10.2±1.8	2.8±0.5	0.21±0.06	0.4±0.1	3.2±0.7	0.89±0.05
82.8 [13, p.w.]	13.4±1.3	2.8±0.8	0.17±0.05	0.92±0.14	3.4±1.1	0.79±0.08
118 [29]	21.3±1.0	6.0±0.6	0.22±0.02			
119 [14,15]	17.3±2.0	4.4±0.6	0.20±0.04	1.1±0.2	4.0±0.6	0.78±0.06
162 [14,15]	19.6±2.7	6.0±0.8	0.23±0.05	0.8±0.2	5.0±0.6	0.86±0.04
162 [29]	17.4±0.8	7.2±0.7	0.29±0.03			
165 [17]	17.0±2.6	9.2±2.3	0.35±0.09	0.91±0.20	4.2±1.2	0.82±0.07
206 [14,15]	13.0±1.7	2.5±0.6	0.16±0.05	0.9±0.2	4.0±0.7	0.82±0.06
239 [29]	7.0±0.6	3.0±0.5	0.30±0.05			
350 [16,32]	2.19±0.19	1.53±0.27	0.41±0.06	0.6±0.2		
		1.80±0.16	0.45±0.05			
500 [32]	0.72±0.07	0.51±0.08	0.41±0.06			
		0.64±0.08	0.47±0.06			

nature in the form of a peak in the quantity $m_x^2=(T_2+T_3)^2-(p_2+p_3)^2$. We checked this quantity in our data (the kinetic energies T_i and momenta p_i are measured in the experiment) at $3N$ absorption configurations. No peak was found. For HFSI, one of the two on-shell nucleons from $2N$ absorption interacts with the third (former spectator) nucleon. The second nucleon of the initial $2N$ absorption emerges with the energy it obtained in the $2N$ absorption process. Therefore, HFSI should be seen experimentally in the form of a peak in T_1 (the energy of the proton detected in the telescope) at the $2N$ absorption energy, with the other two nucleons sharing the remaining energy (in contrast to $2N$ absorption). Again, no peak of this kind was seen at $3N$ configurations.

Weber *et al.* [15], following Fasano and Lee [45], suggest a two-step process in which two nucleons, after absorbing the pion, form a six-quark bag. This bag interacts with the third nucleon leading to $3N$ absorption. The six-quark bag is expected to be long lived as it can achieve quantum numbers which prohibit it from decaying to two nucleons. With all three nucleons involved in the last reaction step, this process should have phase-space-like behavior.

A genuine $3N$ absorption process was suggested by Ashery [46] and followed by Mateos and Šimičević [47]. The model is analogous to the two-nucleon absorption mechanism which can be described as $\pi NN\rightarrow\Delta N\rightarrow NN$. For the $3N$ absorption mechanism an intermediate πNN resonance is assumed to play the role of the Δ in the $2N$ absorption process: $\pi NNN\rightarrow(\pi NN)N\rightarrow NNN$. The predictions of this model are in good agreement with the data although more detailed comparisons are needed in order to determine the role of this mechanism in $3N$ pion absorption.

C. Final-state interaction

The cross section for π^+ absorption via FSI, $\sigma_{\mathrm{FSI}\pi^+}=2.4\pm0.7$ mb, indicates that at 37.0 MeV the FSI process is of the same order of magnitude as the $3N$ absorption process (1.3 ± 0.3 mb). The factor between data and phase space was observed to be up to 20 times higher at angles with FSI influence than elsewhere. On the other hand, the angular range of the FSI is small, whereas the $3N$ absorption occupies the whole region allowed by phase space. The combination of these two effects makes the above result for the FSI very plausible. The same is true for π^-, where the estimated result of the summed LE and HE FSI peaks (0.7 ± 0.2 mb) is about half the value measured for $3N$ absorption (1.6 ± 0.7 mb). The similarity in shape of the π^- $2N$ and FSI differential cross section distributions is remarkable (Figs. 9 and 12). However, theoretical calculations relating these two processes are not available.

D. Pion absorption and photodisintegration

There is interest in comparing pion absorption and photodisintegration. For heavy targets, photon induced reactions are more sensitive to the nuclear interior compared to the strongly absorbed pion probe. In ^{3}He this is not the case and the comparison can be more sensitive to the intrinsic differences between the two probes. The spectra for both γ and π induced reactions on ^{3}He contain $2N$, $3N$ phase space and FSI contributions [48,49]. The technique of incoherent separation of $2N$ and $3N$ absorption was used also successfully by d'Hose *et al.* [50]. Higher energy γ data are now available from Suda *et al.* and Emura *et al.* [51]. Data with polarized γ rays are available from Ruth *et al.* [52], and Tedeschi *et al.* [53]. Calculations of $\gamma+(pn)$ and $\gamma+(pp)$ $2N$ photodisintegration in ^{3}He are being carried out by Niskanen, Wilhelm, and Arenhövel [54,55], also with Fadeev wave functions. The consistency of their approach is tested by comparison to both γ and pion data.

VI. CONCLUSIONS

We measured π^+ absorption on quasideuterons and π^- absorption on diprotons at $T_\pi=37.0$ MeV using

^{3}He(π^+,pp)p and ^{3}He(π^-,pn)n, respectively. In addition, we measured the $3N$ and FSI absorption of π^+ and π^- on ^{3}He at $T_\pi = 37.0$ MeV, and reevaluated the $3N$ absorption at $T_\pi = 62.5$ and 82.8 MeV using the data of Aniol *et al.* [13].

The experimental results of the π^+ absorption on a quasideuteron at 37.0 MeV show consistency with results of experiments carried out earlier at higher energies.

The energy dependence of the total cross sections, over the energy range from 37 to 500 MeV, follows the Δ resonance. The absorption through an intermediate ΔN state is still dominant at 37.0 MeV. The ratio $\sigma(2N,\pi^+)/\sigma(2N,\pi^-)$ is close to 10 (compared to ≈ 20 at the peak of the Δ resonance, and <4 at 350 MeV).

As a consequence of the dominance of the Δ, the ratio of the $2N$ absorption $\sigma(\pi^{+3}\mathrm{He})/\sigma(\pi^+ d)$ at this energy is 1.5 as throughout the Δ resonance energy region.

The dominance of the p-wave pion channel is reflected in the ratio $A_2/A_0 = 0.95 \pm 0.09$. The slight deviation from unity is an indication of s-wave pions beginning to contribute at this energy, in agreement with observations of pion absorption on the deuteron at low energies [26].

The results of π^- absorption on the diproton are consistent with the results at higher energies in the following points.

The total cross sections, over the energy range from 37 to 350 MeV, are nearly constant at about $\sigma = 0.8 \pm 0.2$ mb.

The angular distribution of the differential cross sections is asymmetric (backward peaked) at all energies measured so far (37–350 MeV).

The asymmetry increases with decreasing energy, and reaches its largest value measured so far at 37.0 MeV ($A_1/A_0 = -1.04 \pm 0.07$).

The minimum in the angular distribution of $d\sigma/d\Omega$ shows a systematic shift to smaller angles, with lower pion beam energies.

The relative strength of the pion s wave increases at $T_\pi = 37.0$ MeV. From a partial wave amplitude analysis, it is calculated to be 0.13. This increase causes the observed increase in asymmetry (shift of the minimum) of the angular distribution. This strength makes the present data particularly useful to study heavy meson exchange and short range correlations.

The main results for the $3N$ absorption process at 37.0 MeV are the following.

The total cross sections for π^+ and π^- are of similar magnitude, as observed at higher energies.

In the energy range 63–119 MeV, the $3N$ cross sections are nearly constant, for both π^+ and π^-. Compared to the cross sections at these energies, the π^+ and π^- $3N$ cross sections at 37.0 MeV drop by a factor of 2 to 3. Consequently, the ratio $\sigma_{3N}/(\sigma_{2N}+\sigma_{3N})$ drops at 37.0 MeV (π^+ and π^-). A drop in the $3N$ cross sections at low energies is expected from the observation that for stopped pions the $3N$ phase space region is virtually empty [24].

Related to this observation is the increase in the ‘‘soft’’ final-state interaction (two nucleons recoiling together back to back against the third) at 37.0 MeV. For stopped pions, ‘‘collinear’’ events ($2N$ and soft FSI) made up for all the events observed. This trend becomes visible at 37.0 MeV, where the FSI cross sections are of the same order of magnitude as the $3N$ cross sections (π^+ and π^-).

The relative strength of the two-pion p-wave subchannels ($^3S_1$ and $^3D_1$) in the π^- $2N$ absorption process can be tested by measuring the polarization of one of the nucleons in the final state. Such measurements via the inverse reaction at corresponding proton beam energies [19–21] give preference to the ‘‘S’’ solution (Fig. 11, Table VIII). The absorption experiments of the present work at 37.0 MeV and of Aniol *et al.* [13] at 62.5 and 82.8 MeV, combined with the polarization measurements mentioned, provide a complete data base. This data base should enable and encourage further theoretical calculations for the understanding of the mechanisms involved in pion absorption on a diproton $^1S_0$ pair, and of details of the diproton wave function in ^{3}He. In particular, it should allow tests of different models, such as boson exchange (including heavy meson exchange) and six-quark bags, or their combination.

ACKNOWLEDGMENTS

The support of E. Vogt and the TRIUMF management is acknowledged by the Tel Aviv University collaborators. We thank R. Redwine for useful discussions. We thank J. Vincent for construction and maintenance of the liquid ^{3}He target, and E. Cochavi and Z. Hermon for assistance during data taking. This work was supported in part by the US-Israel Binational Science Foundation.

---

[1] H. J. Lipkin, Phys. Lett. B **198**, 131 (1987).
[2] J. A. Niskanen and A. W. Thomas, Phys. Lett. B **196**, 299 (1987).
[3] R. Schiavilla, D. S. Lewart, V. R. Pandharipande, S. C. Pieper, R. B. Wiringa, and S. Fantoni, Nucl. Phys. **A473**, 267 (1987).
[4] H. de Vries, C. W. de Jager, and C. de Vries, At. Data Nucl. Data Tables **36**, 495 (1987).
[5] K. Ohta, M. Thies, and T.-S. H. Lee, Ann. Phys. (NY) **163**, 420 (1985).
[6] D. Ashery, Nucl. Phys. **A478**, 603 (1988), and references therein.
[7] M. Steinacher, G. Backenstoss, M. Izycki, P. Salvisberg, P. Weber, H. J. Weyer, A. Hoffart, B. Rzehorz, H. Ullrich, D. Dzemidzić, M. Furić, and T. Petković, Nucl. Phys. **A517**, 413 (1990), and references therein.
[8] E. M. Nyman and D. O. Riska, Phys. Lett. B **215**, 29 (1988).
[9] C. J. Horowitz, H. O. Meyer, and D. K. Griegel, Phys. Rev. C **49**, 1337 (1994).
[10] S. MayTal-Beck, J. Aclander, A. Altman, D. Ashery, H. Hahn, M. A. Moinester, A. Rahav, A. Feltham, G. Jones, M. Pavan, M. Sevior, D. Hutcheon, D. Ottewell, G. R. Smith, and J. A. Niskanen, Phys. Rev. Lett. **68**, 3012 (1992).
[11] J. Aclander, S. MayTal-Beck, A. Altman, D. Ashery, H. Hahn, M. A. Moinester, A. Rahav, A. Feltham, G. Jones, M. Pavan,

M. Sevior, D. Hutcheon, D. Ottewell, G. R. Smith, and J. A. Niskanen, Phys. Lett. B **300**, 19 (1993).

[12] M. A. Moinester, D. R. Gill, J. Vincent, D. Ashery, S. Levenson, J. Alster, A. Altman, J. Lichtenstadt, E. Piasetzky, K. A. Aniol, R. R. Johnson, H. W. Roser, R. Tacik, W. Gyles, B. Barnett, R. J. Sobie, and H. P. Gubler, Phys. Rev. Lett. **52**, 1203 (1984).

[13] K. A. Aniol, A. Altman, R. R. Johnson, H. W. Roser, R. Tacik, U. Wienands, D. Ashery, J. Alster, M. A. Moinester, E. Piasetzky, D. R. Gill, and J. Vincent, Phys. Rev. C **33**, 1714 (1986).

[14] P. Weber, G. Backenstoss, M. Izycki, R. J. Powers, P. Salvisberg, M. Steinacher, H. J. Weyer, S. Cierjacks, A. Hoffart, H. Ullrich, M. Furić, T. Petković, and N. Šimičević, Nucl. Phys. **A501**, 765 (1989).

[15] P. Weber, G. Backenstoss, M. Izycki, R. J. Powers, P. Salvisberg, M. Steinacher, H. J. Weyer, S. Cierjacks, A. Hoffart, B. Rzehorz, H. Ullrich, D. Bosnar, M. Furić, T. Petković, and N. Šimičević, Nucl. Phys. **A534**, 541 (1991).

[16] L. C. Smith, R. C. Minehart, D. Ashery, E. Piasetzky, M. Moinester, I. Navon, D. F. Geesaman, J. P. Schiffer, G. Stephans, B. Zeidman, S. Muhkopadhyay, R. E. Segel, M. Sabar, B. Anderson, R. Madey, and J. Watson, in *Pion Absorption in* ^{3}*He at 350 MeV*, Proceedings of the Eleventh International Conference on Particles and Nuclei (Contributed Papers), Kyoto, Japan, 1987, edited by S. Homma *et al.* (North-Holland, Amsterdam, 1988), p. 338.

[17] S. Mukhopadhyay, S. Levenson, R. E. Segel, G. Garino, D. Geesaman, J. P. Schiffer, G. Stephans, B. Zeidman, E. Ungricht, H. Jackson, R. Kowalczyk, D. Ashery, E. Piasetsky, M. Moinester, I. Navon, L. C. Smith, R. C. Minehart, G. S. Das, R. R. Whitney, R. Mckeown, B. Anderson, R. Madey, and J. Watson, Phys. Rev. C **43**, 957 (1991).

[18] E. Piasetzky, D. Ashery, M. A. Moinester, G. A. Miller, and A. Gal, Phys. Rev. Lett. **57**, 2135 (1986).

[19] C. Ponting, D. A. Hutcheon, M. A. Moinester, P. L. Walden, D. R. Gill, R. R. Johnson, F. Duncan, G. Sheffer, P. Weber, V. Sossi, A. Feltham, M. Hanna, R. Olszewski, M. Pavan, F. M. Rozon, M. Sevior, D. Ashery, R. P. Trelle, H. Hahn, and B. Mayer, Phys. Rev. Lett. **63**, 1792 (1989).

[20] F. Duncan, Ph.D. thesis, University of British Columbia, 1993; F. Duncan *et al.*, unpublished.

[21] H. Hahn, Ph.D. thesis, Tel Aviv University, 1993; H. Hahn *et al.*, unpublished.

[22] E. Jans, P. Barreau, M. Bernheim, J. M. Finn, J. Morgenstern, J. Mougey, D. Tarnowski, S. Turck-Chieze, S. Frullani, F. Garibaldi, G. P. Capitani, E. de Sanctis, M. K. Brussel, and I. Sick, Phys. Rev. Lett. **49**, 974 (1982).

[23] E. Jans, M. Bernheim, M. K. Brussel, G. P. Capitani, E. de Sanctis, S. Frullani, F. Garibaldi, J. Morgenstern, J. Mougey, D. Tarnowski, I. Sick, and S. Turck-Chieze, Nucl. Phys. **A475**, 687 (1987).

[24] D. Gotta, M. Dörr, W. Fetscher, G. Schmidt, H. Ullrich, G. Backenstoss, W. Kowald, I. Schwanner, and H.-J. Weyer, Phys. Lett. **112B**, 129 (1982).

[25] E. Friedman, A. Goldring, G. J. Wagner, A. Altman, R. R. Johnson, O. Meirav, and B. K. Jennings, Nucl. Phys. **A514**, 601 (1990).

[26] B. G. Ritchie, R. D. Edge, D. J. Malbrough, B. M. Preedom, F. E. Bertrand, E. E. Gross, F. E. Obenshain, J. R. Wu, M. Blecher, K. Gotow, R. L. Burman, R. Carlini, M. E. Hamm, M. J. Leitch, and M. A. Moinester, Phys. Rev. C **24**, 552 (1981); **26**, 2337(E) (1982).

[27] D. F. Measday and C. Richard-Serre, Nucl. Instrum. Methods **76**, 45 (1969).

[28] R. A. Cecil, B. D. Anderson, and R. Madey, Nucl. Instrum. Methods **161**, 439 (1979).

[29] T. Alteholz, D. Androić, G. Backenstoss, D. Bosnar, H. Breuer, A. Brković, H. Döbbeling, T. Dooling, W. Fong, M. Furić, P. A. M. Gram, N. K. Gregory, J. P. Haas, A. Hoffart, C. H. Q. Ingram, A. Klein, K. Koch, J. Köhler, B. Kotlínski, M. Kroedel, G. Kyle, A. Lehmann, Z. N. Lin, G. Mahl, A. O. Mateos, K. Michaelian, S. Mukhopadhyay, T. Petković, R. P. Redwine, D. Rowntree, R. Schumacher, U. Sennhauser, N. Šimičević, F. D. Smit, G. van der Steenhoven, D. R. Tieger, R. Trezeciak, H. Ullrich, M. Wang, M. H. Wang, H. J. Weyer, M. Wildi, and K. E. Wilson, Phys. Rev. Lett. **73**, 1336 (1994).

[30] H. Hahn, M.Sc. thesis, Tel Aviv University, 1987.

[31] R. Hagedorn, *Relativistic Kinematics* (Benjamin, New York, 1963).

[32] L. C. Smith, R. C. Minehart, D. Ashery, E. Piasetzky, M. Moinester, I. Navon, D. F. Geesaman, J. P. Schiffer, G. Stephens, B. Zeidman, S. Levinson, S. Muhkopadhyay, R. E. Segel, B. Anderson, R. Madey, J. Watson, and R. R. Whitney, Phys. Rev. C **40**, 1347 (1989).

[33] H. J. Weyer, Phys. Rep. **195**, 295 (1990).

[34] R. A. Arndt, L. D. Roper, R. A. Bryan, R. B. Clark, B. J. VerWest, and P. Signell, Phys. Rev. D **28**, 97 (1983); R. A. Arndt, L. D. Roper, R. L. Workman, and M. W. McNaughton, Phys. Rev. D **45**, 3995 (1992); R. A. Arndt *et al.*, (SAID) program, Virginia Polytechnic Institute, 1988, via telnet to VTINTE.PHYS.VT.EDU, with login (password) PHYSICS (QUANTUM).

[35] O. V. Maxwell and C. Y. Cheung, Nucl. Phys. **A454**, 606 (1986).

[36] G. A. Miller and A. Gal, Phys. Rev. C **36**, 2450 (1987).

[37] M. Bachman, P. Riley, and C. Hollas, Phys. Rev. C **42**, 1751 (1990).

[38] J. Dubach, W. M. Kloet, and R. R. Silbar, Nucl. Phys. **A466**, 5753 (1987).

[39] J. A. Niskanen, Phys. Rev. C **43**, 36 (1991).

[40] H. O. Meyer, C. Horowitz, H. Nann, P. V. Pancella, S. F. Pate, R. E. Pollok, B. von Przewoski, T. Rinckel, M. A. Ross, and F. Sperisen, Nucl. Phys. **A539**, 633 (1992).

[41] T.-S. H. Lee and D. O. Riska, Phys. Rev. Lett. **70**, 2237 (1993).

[42] J. A. Niskanen, Phys. Rev. C **49**, 1285 (1994).

[43] J. A. Niskanen, private communication.

[44] L. L. Salcedo, E. Oset, D. Strottmann, and E. Hernández, Phys. Lett. B **208**, 339 (1988).

[45] C. Fasano and T.-S. H. Lee, Phys. Lett. B **217**, 9 (1989).

[46] D. Ashery, Phys. Rev. C **36**, 460 (1987).

[47] A. Mateos and N. Šimičević, Phys. Rev. C **47**, 1842 (1993).

[48] N. R. Kolb, P. N. Dezendorf, M. K. Brussel, B. B. Ritchie, and J. H. Smith, Phys. Rev. C **44**, 37 (1991).

[49] A. J. Sarty, K. G. R. Doss, G. Feldman, E. L. Hallin, R. E. Pywell, G. A. Retzlaff, D. M. Skopik, H. R. Weller, W. R. Dodge, J. W. Lightbody, J. S. O'Connell, and C. C. Chang, Phys. Rev. C **47**, 459 (1993).

[50] N. d'Hose G. Audit, A. Bloch, N. de Botton, L. Jammes, J. M. Laget, J. Martin, E. Mazzucato, A. Sasaki, C. Schuhl, G. Tamas, L. Ghedira, M. Rodgers, P. Stoler, P. Argan, and P. Pedroni, Phys. Rev. Lett. **63**, 856 (1989).

[51] T. Suda, *Photon Absorption by Two Protons in He3*, Proceedings of the Invited Talk at the 6th workshop on Perspectives in Nuclear Physics at Intermediate Energy (ICTP, Trieste, Italy, 1993); T. Emura *et al.*, Phys. Rev. C **49**, 597 (1994).

[52] C. Ruth, G. S. Adams, H. Baghaei, A. Caracappa, W. B. Clayton, A. D'Angelo, M.-A. Duval, G. Giordano, S. Hoblit, O. C. Kistner, J. M. Laget, R. Lindgren, G. Matone, L. Miceli, W. K. Mize, M. A. Moinester, A. M. Sandorfi, C. Schaerf, R. M. Sealock, L. C. Smith, P. Stoler, D. J. Tedeschi, P. K. Teng, C. E. Thorn, S. T. Thornton, K. Vaziri, C. S. Whishnant, and E. J. Winhold, Phys. Rev. Lett. **72**, 617 (1994).

[53] D. J. Tedeschi, G. S. Adams, G. Audit, H. Baghaei, A. Caracappa, W. B. Clayton, A. D'Angelo, M.-A. Duval, G. Giordano, S. Hoblit, O. C. Kistner, J. M. Laget, R. Lindgren, G. Matone, L. Miceli, W. K. Mize, M. Moinester, C. Ruth, A. Sandorfi, C. Schaerf, R. M. Sealock, L. C. Smith, P. Stoler, P. K. Teng, C. E. Thorn, S. T. Thornton, K. Vaziri, C. S. Whishnant, and E. J. Winhold, Phys. Rev. Lett. **73**, 408 (1994).

[54] J. A. Niskanen, P. Wilhelm, and H. Arenhövel, Nucl. Phys. **A586**, 693 (1995); P. Wilhelm, J. A. Niskanen, and H. Arenhövel, Phys. Lett. B **335**, 109 (1995).

[55] P. Wilhelm, H. Arenhövel, and J. A. Niskanen, Phys. Rev. Lett. **74**, 1034 (1995); P. Wilhelm, J. A. Niskanen, and H. Arenhövel, Phys. Rev. C **51**, 2841 (1995).